Selecting genes for analysis using historically contingent progress: from RNA changes to protein-protein interactions

Farhaan Lalit[1], Antony M Jose[1]*

Affiliations:

[1]University of Maryland, College Park, MD, USA.

*Corresponding author. Email: amjose@umd.edu

Author Contributions: A. M. J. designed the study; F. L. and A. M. J. performed the analyses (F. L. - all work on data tables and A. M. J. - all work on AlphaFold-based analyses); and F. L. and A. M. J. wrote the paper.

Competing Interest Statement: The authors declare no competing interests.

Keywords: Mutual Information, AlphaFold, RNA silencing, homeostasis, *C. elegans*.

Abstract

Progress in biology has generated numerous lists of genes that share some property. But advancing from these lists of genes to understanding their roles is slow and unsystematic. Here we use RNA silencing in *C. elegans* to illustrate an approach for prioritizing genes for detailed study given limited resources. The partially subjective relationships between genes forged by both deduced functional relatedness and biased progress in the field was captured as mutual information and used to cluster genes that were frequently identified yet remain understudied. Some proteins encoded by these understudied genes are predicted to physically interact with known regulators of RNA silencing, suggesting feedback regulation. Predicted interactions with proteins that act in other processes and the clustering of studied genes among the most frequently perturbed suggest regulatory links connecting RNA silencing to other processes like the cell cycle and asymmetric cell division. Thus, among the gene products altered when a process is perturbed could be regulators of that process acting to restore homeostasis, which provides a way to use RNA sequencing to identify candidate protein-protein interactions. Together, the analysis of perturbed transcripts and potential interactions of the proteins they encode could help prioritize candidate regulators of any process.

Introduction

Genes and gene products are often collected as lists based on unifying characteristics or based on experiments. Examples include genes that show enrichment of a chromatin modification, mRNAs that change abundance in response to a mutation, and proteins that interact with another protein. After the initial identification of a set of genes as belonging to a list, multiple approaches (1) are needed to generate an explanatory model. However, many genes do not receive further attention, as evidenced by recent meta-analyses, which highlighted numerous understudied genes in humans (2,3). Since single publications often analyze only one or a few genes, a wider view of genes with roles in a process could be gained by comparing lists generated by several studies. Such exploration could identify genes that are present in multiple lists but have not yet been selected for detailed study. Identifying these understudied genes is especially useful during the early stages of a field, when coherent models for most observed phenomena have not yet emerged. While this approach is also extensible to lists of anything that is used to characterize living systems (changes in lipids, metabolites, localizations, etc.), here we focus on lists of mRNAs, proteins, and small RNAs generated by the field of RNA silencing in the nematode *C. elegans*.

A gene present in many lists could be regulated in multiple separable ways and/or be regulated in one or a few ways by connected sets of regulators (Fig. 1*A*). For example, mRNA levels could be regulated through changes in transcription, turnover, localization, small RNA production, etc. or all changes could occur because of turnover regulation by a connected set of regulators. Changes in such genes could alter specific regulatory outputs, making them integrators of inputs from many other regulators. Alternatively, they could have no measurable consequence but might still be experimentally useful as general indicators of perturbation. One way that organisms could use general sensing of perturbation in a process could be to return the process to the pre-perturbation state through feedback (4). Such active resetting would enable restoration of homeostasis faster than through the dissipation of the perturbation alone.

Here we present an approach to identify regulated but understudied genes in the field of RNA silencing in *C. elegans*. While these genes could play a variety of roles, we find that some of these genes encode predicted influencers of RNA-regulated expression that can directly interact with key regulators of RNA silencing. Others could serve as regulatory links that connect RNA silencing with other processes. The many hypotheses generated through these analyses need to be evaluated using experiments that selectively perturb regulatory interactions.

Materials and Methods

Data tables from 82 studies on RNA silencing in *C. elegans* that were published between 2007 and 2022 were downloaded (Table S1), reformatted manually and/or using custom scripts, and filtered to generate lists that only include entries with reported p-values or adjusted p-values < 0.05, when such values were available. Gene names were standardized across datasets using tools from Wormbase (5). The top 'g' genes that occur in the greatest numbers of tables were culled as the most frequently identified genes. A measure for the extent of regulation of each gene (r_g) was used to aid their prioritization for detailed study. Co-occurrence patterns of genes in different tables were captured using the Jaccard distance (d_J) (6) or a symmetric measure of normalized mutual information (7), defined here as Historical Mutual Information (HMI). The d_J values were used to generate a dendrogram using the average linkage method (Fig. 1). HMI was used to group genes into clusters according to the Girvan-Newman algorithm (8) and different sets of genes were highlighted (Fig. 8). Gene ontology (GO) analyses were performed using Gene Ontology Resource (https://geneontology.org/; (9,10)).

Prediction of dimer formation between the 18 proteins encoded by understudied genes among the top 25 genes and 25 key regulators of RNA silencing were obtained using AlphaFold 2 (11,12) run on a high-performance cluster (Zaratan at UMD) and/or using the AlphaFold 3 (13) server online (https://golgi.sandbox.google.com/). Large regulators (DCR-1, EGO-1, ZNFX-1, NRDE-2, and MET-2) were tested on the AlphaFold 3 server initially and positive hits, if any, were examined again using AlphaFold 2 (e.g., interaction of EGO-1 with W09B7.1). The computed models were processed using custom shell scripts, python programs, and ChimeraX (14). Briefly, the highest ranked model for each pair of proteins was depicted with the predicted aligned error used to highlight inter-protein interactions as pseudobonds colored according to the alphafold pae palette on ChimeraX (Movie S1 to S93). For models that satisfy the criteria for maxPae (<5 Å) and for distance (<6 Å), an approximation of the interaction area was calculated by isolating the mutually constrained residues and using the 'buriedarea' command (ChimeraX). This area was divided by the product of the number of amino acids in each protein to get a normalized value and scaled uniformly before plotting (e.g., Fig. 2*B*). Finally, the ranking scores (0.8*ipTM + 0.2*pTM for AlphaFold 2.3 and 0.8*ipTM + 0.2*pTM + 0.5*disorder for AlphaFold 3) were used to shade the circle representing each interaction (Fig. 2*B*) and/or plotted (Fig. 5*A*). All interactions predicted in the study were summarized into a network diagram (Fig. 8*G*) using Gephi and Adobe Illustrator.

See Supplemental Material for detailed materials and methods.

Results

Many genes have been repeatedly reported within data tables but remain understudied.

To determine if there are any understudied regulated genes that are relevant for RNA silencing in *C. elegans*, we examined data from past studies in the field. While complete replication of each study might be needed for direct comparisons, this goal is impractical. Even beginning with the 'raw' data deposited to public resources (e.g., fastq files after RNA-seq) and repeating the analyses reported in a publication is not always feasible. Summary tables from previous analyses presented in publications provide a practical intermediate level of data to use for comparisons across studies. Therefore, we collated a total of 398 tables from 82 publications for comparison (see methods and Table S1 for list of tables) and joined the tables together after standardizing gene names to yield genes that can be compared for presence or absence across the 398 lists (Fig. 1*B*). About 86% (342 of 398) of the included gene lists document RNA changes (mRNA, small RNA, or total RNA) that accompany a perturbation. Of the remaining ~14%, some lists document co-immunoprecipitating proteins (19), were pre-defined enrichment lists (24), or are based on other experiments (13). To prioritize a set of genes (g) that receive extensive regulatory input and/or that encode proteins that interact with many other proteins and are yet

included in selective lists, we propose a metric r_g (Fig. 1*B*). Since the likelihood of including a gene from the lists increases with g, the metric is specified with a subscript for each analysis (e.g., r_{25} refers to a regulation score when the top 25 genes that are most commonly present in lists are considered) and defined to be:

$$r_g := \sum_{i=1}^{n} \frac{S_i}{T_i}$$

where g = size of gene set chosen for analysis, n = total number of lists with altered genes, S_i = number of genes from the i^{th} list that is also present in the gene set g, and T_i = total number of genes in the i^{th} list. The larger the set of genes (g) selected, the greater the chance of a dataset (with T_i genes) having at least one overlapping gene within the selected gene set (probability given by $P(S_i > 0)$ in Fig. 1*C*). The metric r_g is a decision aid that helps with choosing genes for experimental analysis and is not to be taken as an objective measure of the importance of the gene for the biological process under study.

The top 25 genes sorted according to their r_{25} values included the germline Argonaute HRDE-1 (15), which has been the subject of numerous studies (Fig. 1*D*). While most other genes are understudied (fewer than 10 publications on WormBase), among the 25 genes is *sdg-1*, which was recently reported to be regulated by the double-stranded RNA (dsRNA) importer SID-1 and encodes a protein with a suggested role in feedback regulation of heritable RNA silencing by colocalizing with perinuclear germ granules (16). This discovery suggests that the analysis of the additional genes with high r_{25} values could also be fruitful. Of the 18 understudied genes that encode proteins, seven had predicted structures of high confidence (i.e., domains with predicted local distance difference test (pLDDT) > 90) in the AlphaFold Protein Structure Database (12). These structures were then used to identify related protein domains using Foldseek (17) (Fig. 1*E*; E-value < 0.05). These include conserved domains, most of which have known biochemical activities: de-ubiquitinase (E01G4.5), SPK (C08F11.7), aspartic protease (K02E2.6), RNAse H1 (RNH-1.3), F-box B (FBXB-97), BTB plus MATH (BATH-45), and RNA Recognition Motif (R06C1.4). Three more proteins have been proposed to be nucleocapsid-like proteins encoded by genes within retrotransposons ((16,18); F15D4.5, C38D9.2, and W09B7.1 in Fig. 1*E*). These candidates can be experimentally analyzed in the future for possible roles in RNA silencing. To explore the relationships between these genes (Fig. 1*F* and 1*G*), we clustered the genes and generated a dendrogram where genes present together in different lists are closer together (see supplementary methods). The dendrogram had a cluster (red in Fig. 1*G*) that included all four pseudogenes, suggesting that this method could capture functional relatedness despite the limitations and biases introduced by the available data.

Multiple proteins encoded by the top 25 genes are predicted to interact with known regulators of RNA silencing.

In general, understudied regulated genes could play diverse roles, some of which could impact RNA silencing. Such feedback during RNA silencing is supported by recent observations. For example, animals typically recover from silencing initiated by dsRNA within the germline (19) or in somatic cells (20). This recovery occurs despite the presence of amplification mechanisms, suggesting that silencing ends either when the trigger dsRNA runs out and/or because of homeostatic control through feedback inhibition. In support of self-limiting behavior that is expected upon feedback inhibition, an inhibitor of RNA silencing is recruited to genes targeted by dsRNA (21) and a regulatory loop limits the production of some endogenous small RNAs (22). Some of the top understudied regulated genes identified here could play a role in the homeostatic return after perturbation. The return could be achieved by modulating the activity of factors that promote RNA silencing in a variety of ways, including regulation of transcription, post-

transcriptional RNA processing, RNA localization, translation, post-translational modifications on proteins, protein localization, etc. Of these possibilities, one that could be surveyed computationally is regulation through direct protein-protein interactions. Therefore, to test if any of the proteins encoded by the top 25 genes could interact with known regulators of RNA silencing, we examined the potential for protein-protein interactions using their predicted structures.

We selected 25 known regulators of RNA silencing (see Fig. 2*A*) chosen for their roles in different phases of the deduced mechanism(s) of RNA silencing (23-25). These include proteins with roles in the processing of dsRNA and its regulators; Argonaute proteins and their regulators; proteins with roles in secondary small RNA production and its regulators; components of germ granules; and co-transcriptional regulators (Fig. 2*A*). We then examined their predicted interactions with the 18 proteins encoded by understudied regulated genes among the top 25 (highlighted in red, Fig. 1*G*). For 20 RNA regulators, we used AlphaFold 2, which makes extensive use of multiple sequence alignments for computing inter-protein interactions and has a success rate of ~50-60% (26,27). Since the computational cost of AlphaFold 2 escalates with the number of amino acids, interactions with the remaining 5 larger regulators (DCR-1, EGO-1, ZNFX-1, NRDE-2, and MET-2) were tested on the recently available but proprietary AlphaFold 3 server (13), which can predict interactions with ligands, and as with AlphaFold 2, uses multiple sequence alignments for its structure predictions. To stratify the predicted interactions, we initially considered the maximal inter-protein predicted aligned error (PAE) and the distance between the interacting residues (distance), which was allowed to be up to twice the length of hydrogen bonds (~3 Å (28)). Examining interactions with a criterion of PAE less than 5 (which is more stringent than the 8 Å error that has been used successfully (29)) revealed numerous interactions (blue in Fig. 2*B*). Therefore, to constrain the predictions further, we used the ranking scores, which are a combination of interface-predicted template modeling (ipTM) and predicted template modeling (pTM) scores: 0.8*ipTM + 0.2*pTM for AlphaFold 2.3 (11) and 0.8*ipTM + 0.2*pTM + 0.5*disorder for AlphaFold 3 (13). We only considered interactions with a ranking score greater than 0.6, which is relatively high given than ipTM scores as low as ~0.3 can yield true positives (30), and that constrain a minimum of 20 residues in the proteins encoded by understudied genes (not grey in Fig. 2*B*), which we define as predicted interactions of high confidence. Together, these criteria identified 32 interactions (Fig. 2*B* and Movies S1 to S32). Among the regulators, RDE-3 and RDE-8 had the highest numbers of predicted interactors (5 proteins each) and among the proteins encoded by understudied genes, FBXB-97 had the highest number of predicted interactors (7 proteins). These high-confidence interactors included proteins that were predicted to interact with every phase of the deduced mechanism(s) for RNA silencing (Fig. 2*C*). Since the precise numbers of interacting residues required for a meaningful interaction in vivo is variable and unknown, interactions that constrain fewer residues could have measurable impacts on function. Nevertheless, we conservatively designate each protein that is predicted to interact with one or more RNA regulators with relatively high confidence as a **P**redicted **I**nfluencer of **R**NA-regulated **E**xpression (PIRE). We refer to five of these as PIRE-1 through PIRE-5 (Y20F4.4, C08F11.7, E01G4.5, F15D4.5, and K02E2.6, respectively; Fig. 2*D*) and preserve the names of the four that were already given names based on structural homology (subunit of the **T**ranslocase of the **I**nner **M**itochondrial **M**embrane TIMM-17B.2, the **F**-**b**o**x B** protein FBXB-97 and the **RN**ase **H** protein RNH-1.3) or after detailed study (the **S**ID-1-**d**ependent **g**ene protein SDG-1). For convenience, these nine putative interactors (and any additional interactors identified below) are collectively referred as PIRE proteins here. This provisional designation can be amended should more specific information regarding their roles be obtained through future experimental studies.

Each of these interactions (Fig. 2*B* and Movie S1 to S32) suggest hypotheses for their functional impact based on the known roles of RNA regulators and the domains present in PIRE proteins (Fig. 1*E*). The two PIRE proteins encoded by genes within retrotransposons (PIRE-4 and SDG-1) that also interact with regulators of RNA silencing, supports the idea that retrotransposon-

encoded genes influence their own RNA-mediated regulation (e.g., (16)). FBXB-97, which is predicted to be an F-box protein (31), could promote ubiquitin-mediated degradation of its interactors (RDE-4, ERI-1, NRDE-3, DEPS-1, PID-2, RDE-8, and RDE-3), sequester them (inhibiting their activity), or potentially promote ubiquitination of their interacting RNA (32). A precedent for such an intersection between ubiquitin-mediated protein degradation and small RNA-mediated RNA regulation is the role for a ubiquitin ligase in degrading Argonautes when there is extensive base-pairing between miRNAs and their targets (33,34). PIRE-5, which is predicted to be a protease, could cleave its interactors (ERI-1, PID-2, RDE-8, and SET-25) to regulate their activity – a mode of regulation that has been recently elucidated for Argonaute proteins (35) and implicated in RNA silencing within the germline (36). Additional PIRE proteins with confidently predicted domains (e.g., RNase H in RNH-1.3, multiple domains in PIRE-3, and SPK domain in PIRE-2) potentially implicate new biochemical activities in the process of RNA silencing. In all, two general modes of interaction between PIRE proteins and the tested regulators of RNA silencing that are not mutually exclusive could be discerned (Fig. 3). In one mode exemplified by FBXB-97 (Fig. 3, *left*), the interactions with most regulators involve nearly the same set of residues. In the other mode exemplified by PIRE-3 (Fig. 3, *right*), interactions with different regulators involve different sets of residues. In summary, predictions using AlphaFold identify numerous interactions that inspire follow-up work to test hypotheses about the roles of PIRE proteins in RNA silencing.

Predictions by AlphaFold 2 and AlphaFold 3 do not always agree.

While AlphaFold 2 predicted all the interactions classified as high-confidence interactions, the one interaction predicted by AlphaFold 3 (EGO-1 and W09B7.1) with a maximal PAE <5Å and distance <6Å constrained fewer than 20 residues (Fig. 2*B*, Fig. S1, and Fig. S2). The reason for this extreme discrepancy is unclear.

To directly compare both approaches for predicting protein-protein interactions, we examined some of the interactions predicted by each approach using the other. We first examined significant interactions predicted with a high ranking score according to AlphaFold 2 (> 0.8, Fig. 4*A*). Of these, only the interaction between RNH-1.3 and RDE-3 was confidently predicted by AlphaFold 3, albeit with a lower score (0.85 for AF2 vs 0.68 for AF3). Aligning both predicted complexes using the RDE-3 protein revealed that both predictions are in good agreement (Fig. 4*B* and Movie S33). We next considered two proteins, FBXB-97 and PIRE-4, for which multiple interactors were predicted by AlphaFold 2 with varying confidence. While AlphaFold 2 predicted interactions between PIRE-4 and 3 RNA regulators (ranking = 0.73, 0.70, and 0.61), and between FBXB-97 and 7 RNA regulators (ranking = 0.66, 0.67, 0.75, 0.78, 0.75, 0.77, and 0.76), AlphaFold 3 only predicted an interaction with RDE-3 for both proteins (Fig. 4*C,* ranking = 0.78 and 0.79). The RDE-3-interacting residues of FBXB-97 predicted by both approaches overlapped but those of PIRE-4 did not (Fig. 4*C*). Furthermore, aligning the predicted protein-protein complexes using RDE-3 showed a large discrepancy in the positions of the interacting partners in both cases (Fig. 4*D*, FBXB-97, *left*; PIRE-4, *right*; and Movies S34 and S35). Similarly, comparing the predictions for interactions between EGO-1 and W09B7.1 also revealed large discrepancies (Fig. 4*E* and Movie S36). While a region of interaction was predicted using AlphaFold 3 with PAE <5Å and distance <6Å (Fig. 4*E*, right), regions of interaction were only detectable using AlphaFold 2 when the maximal PAE allowed was increased to 10 (Fig. 4*E*, left). Even at this lower threshold for error, the predicted interacting regions differed between the two approaches (black ovals in Fig. 4*E*).

The reasons for the differences between predictions by AlphaFold 2 and AlphaFold 3 could be varied. For example, differences in sampling of predictions, which is expected to correlate with success rate (37) (25 models per AlphaFold 2 run versus five per AlphaFold 3 run on the server) and/or differences in handling intrinsically disordered regions, for which structures can be identified by AlphaFold 2 if they conditionally fold (38). Modifications to these algorithms

that extend capabilities continue to be developed (e.g., modeling of interacting interfaces within intrinsically disordered regions (39), predicting multiple conformations (40), and predicting large protein assemblies (41)). Therefore, further comparisons as newer algorithms for predicting protein-protein interactions continue to be developed (e.g. (42)) and customized exploration of criteria for interactions (43) may be useful for determining when each algorithm can aid the generation of hypotheses.

Convergence and rarity of models support the use of flexible criteria for initial screens.

The RNH-1.3:RDE-3 complex is supported by relatively high-confidence models predicted using AF 2 and AF 3 (Fig. 4*A* and 4*B*), *rnh-1.3* RNA accumulates in *rde-3(-)* animals (44,45), and both *rnh-1.3* and *rde-3* were featured in the abstract of an early publication (46). Therefore, we examined the predicted interactions between RNH-1.3 and RDE-3 in detail to refine the criteria for identifying candidate interactors and to analyze the potential reasons for differences between predictions by AF 2 and AF 3.

While the high-confidence model of the RNH-1.3:RDE-3 complex by AF 2 had a ranking score of 0.85, all the other 24 models from the run had much lower scores (Fig. 5*A*). In fact, the highest-ranking score in 17 subsequent runs was only 0.51. This rarity of high-scoring models suggests that multiple runs may be required on the AlphaFold 3 server as well to discover the high scoring models. Consistently, only one of 5 new runs of AF 3 resulted in a high-scoring model (Fig. 5*B*). Interestingly, an overlay of models with the top two ranks showed a highly similar structure both in the case of AF 2 and AF 3 predictions despite the large differences in their scores (0.85 vs. 0.51 for AF 2 and 0.74 vs. 0.35 for AF 3 in Fig. 5*C*; and Movies S37 and S38). This observation suggests that for some protein complexes, the models predicted with relatively low ranking scores could nevertheless be close to the highest-scoring model. To systematically analyze the convergence of the models with ranking scores, we overlayed the highest scoring models from the 18 runs of AF 2 and calculated the root mean square deviation (RMSD) of each model from the highest-scoring one (Fig. 5*D*). Scores as low as ~0.4 resulted in models that were within ~4Å RMSD of the highest-scoring model. However, scores below that (red line in Fig. 5D) were associated with models that could either have a low (e.g., < 10Å) or high (e.g., > 20Å) RMSD compared with the highest-scoring model. These analyses suggest that models with a ranking score of 0.4 could be worth exploring further, although we have preserved the more conservative threshold of 0.6 in all subsequent analyses using AlphaFold 2. To make the contributions of the two interacting proteins symmetric, we propose that the product of the number of constrained residues in the bait (n_{bait}) and that in the prey (n_{prey}) be greater than 100. Using these revised criteria, we re-examined all AF 2 predictions (Fig. S3) and found that all 32 previously predicted interactions (Fig. 2B) were preserved, and an additional 10 interactions were predicted as significant (Fig. S3). These additional interactions (Movies S39 to S48) include those of two RNA regulators with R06C1.4 (designated PIRE-6), two RNA regulators with C38D9.2 (designated PIRE-7), and one RNA regulator with T16G12.4 (designated PIRE-8).

Taken together, these analyses suggest heuristics for managing false negatives. Since high-scoring models can be rare (1 in 450 AF 2 models with a score > 0.6 for RNH-1.3:RDE-3) and therefore require many runs to discover, false negative rate can be set based on available computational resources. Given the early convergence of some models with increasing ranking score (a model with ~0.4 ranking score only had an RMSD of ~4Å compared with the highest scoring model for RNH-1.3:RDE-3), reducing the ranking threshold could lead to the discovery of interactors within fewer runs. In contrast, false positives are difficult to estimate or manage because we would need a set of proteins that would not interact with each other under any circumstance – such an idealized set may not exist.

Pseudogenes among the top 25 genes could encode proteins that interact with some RNA regulators.

Since pseudogenes could have the potential to encode peptides, we checked for this possibility in the four identified among the top 25 genes. Examination of all possible reading frames revealed uninterrupted stretches that could code for peptides for each 'pseudogene' (F09E9.7 - 141 aa, W04B5.1 - 85 aa, W04B5.2 - 144 aa, and ZK402.3 - 158 aa). These peptides if expressed have the potential to interact with some of the known RNA regulators tested (6 of 80 possible interactions in Fig. S4; Movies S49 to S54). These could reflect interactions between peptides from these 'pseudogenes' or from the corresponding coding genes. In support of this idea, the STAU-1-like peptide that could be encoded by the 'pseudogene' F39E9.7 and the dsRNA-binding protein STAU-1 (47) are both predicted to interact with ADR-2, CSR-1, and RDE-8 (Fig. S4; Movies S55 to S60). These results highlight the possibility that genes annotated as non-coding RNAs, or pseudogenes could have a role encoding a regulatory peptide.

Multiple predicted interactors of RDE-3 suggest regulated production of poly-UG RNAs.

Currently, information on the interactors of any protein in *C. elegans* is curated at WormBase (5) and the Alliance of Genome Resources (48) websites. We selected the poly-UG polymerase RDE-3, which catalyzes the production of a key intermediate of RNA silencing called poly-UG RNAs (45,49,50), as a case study to examine the value added by analysis using AlphaFold, if any. The websites list 5 physical interactors of RDE-3 identified through experiments reported in multiple publications (MUT-7(51), MUT-16(52), PIK-1(53), PRG-1(54), and RDE-8(55)). Including these putative direct interactors, we tested the interaction of 22 regulators of RNA silencing and found significant interactions with 12 proteins using AF 2 (Fig. 6*A*; Movies S61 to S72). Subsets of proteins appear to constrain different sets of residues on RDE-3 (Fig. 6*B*), suggesting different consequences on RDE-3 activity upon interaction for different groups of proteins. Taken together with the previously discovered interactions, a total of 19 interactors are predicted for RDE-3 by AF 2 (Fig. 6*C*). Of these, only 6 interactors were also identified by AF 3 when searched using 5 different random seeds (Fig. 6*C*). Of these 6, only three identified the same interaction interface (RNH-1.3, PIRE-2, and PIRE-6). Of the previously known and experimentally supported physical interactors, three were identified by AF 2 but not by AF 3 (MUT-16, PIK-1, and RDE-8). Two others (MUT-7 and PRG-1) could not be identified by AF 2 even after five different runs (i.e, among 125 models), suggesting that these are either indirect interactors or require additional multimerization for complex formation. The extensive regulation of RDE-3 suggested by these predicted interactions is consistent with recent experimental results that have revealed differences in the patterns of poly-UG RNAs detected when a germline (45) or somatic gene (20) is targeted by dsRNA, and the diversity of poly-UG patterns associated with different forms of heritable RNA silencing (56).

Predictions after an immunoprecipitation could identify direct links to other processes.

Interactions identified using immunoprecipitation followed by mass spectrometry are likely to be strong interactions with abundant proteins but can be direct or indirect. Immunoprecipitation experiments can also result in large lists of putative interacting proteins (e.g., 365 for CSR-1 in one study (54)), which can make it challenging to prioritize the interactors for further study. Examining candidate interactors using AlphaFold is potentially a way to distinguish direct interactors from indirect interactors or spurious co-precipitates.

To test this possibility, we chose a relatively selective immunoprecipitation experiment that identified 12 putative interactors of the Z-granule surface protein PID-2 (36). Of this dozen, 11 were ~1000 aa or smaller and therefore amenable to testing using AF 2 with reasonable computational resources. Five were identified as significant interactors with the following ranking scores: PID-5 – 0.63, PID-4 – 0.63, KIN-19 – 0.74, PAR-5 – 0.74, and T07C4.3 – 0.53 (Fig. S5*A*;

Movies S73 to S77). Even considering only the 4 proteins that satisfy the more stringent criterion of >0.6 ranking score, this analysis provides useful information. First, it identifies PID-3 and PID-4 as direct interactors in agreement with further experimental evidence provided in the study (36) and predicts the sets of residues constrained by the interactions (Fig. S5*B*), which can be tested using additional experiments. Second, it suggests that KIN-19 and PAR-5 are additional direct interactors. KIN-19 is an ortholog of Casein kinase and was recently shown to phosphorylate the Argonaute ALG-1 (57). The predicted interaction with PID-2 suggests a wider role for this kinase in the regulation of RNA silencing, potentially through the phosphorylation of PID-2 or other substrates localized near Z granules. PAR-5 is a 14-3-3 protein required for the proper partitioning of cytoplasmic components in the early embryo (58). Furthermore, PAR-5 does not show a significant interaction with 19 other tested regulators of RNA silencing after one AF 2 run (Fig. 7*A*), is frequently identified as interacting with PID-2 by AF 2 (Fig. 7*B*), and has an extensive interaction interface (Fig. 7*C*) that constrains the C-terminal 17 amino acids of PID-2 (Fig. 7*D*). Underscoring the high confidence in this interaction, the same interaction is also predicted by AF 3 (Fig. 7*E* and Movie S78) and the **R**GF**S**$_{450}$EC**P** sequence within the interaction domain is close to a consensus (RxxpSxP) for binding 14-3-3 domains (59) with S_{450} phosphorylated by an atypical Protein Kinase C (60). Nevertheless, determining if, when, and where any predicted interactions occur in vivo will require many future experiments.

Some predicted interactions could be challenging to demonstrate experimentally.

Obtaining experimental support for direct interactions between proteins can be difficult. For example, an interaction between the most abundant Gα protein in the brain (Gα_o (61), GOA-1 in *C. elegans*) and the diacylglycerol kinase DGK-1 is strongly predicted by genetic analysis (62,63). Both AF 2 and AF 3 predict the same extensive binding between GOA-1 and DGK-1 (Fig. S6 and Movie S79). Furthermore, the interaction interface is largely preserved and reliably predicted by AlphaFold 3 when GOA-1 is by itself or bound to either GTP or GDP (Fig. S6 and Movie S79). Yet, early attempts using purified proteins failed to reveal a detectable interaction between DGK-1 and GOA-1 in vitro (64), and this interaction has remained a conjecture for more than two decades.

While biochemical approaches rely on preserving or recreating in vitro the unknown conditions in vivo to coax a detectable interaction between proteins, prediction algorithms that incorporate extensive multiple sequence alignments (e.g., AF 2 and to an unknown extent AF 3) can use the co-evolution of residues to deduce the interaction. Given these complementary strengths, systematic analyses using both multiple experimental approaches (1) and multiple prediction algorithms are needed to find the edge of predictability for protein-protein interactions.

The top 100 genes include many that could link RNA silencing to other processes.

To examine if the observations above would hold when analyzing a larger set of genes, we examined the top 100 genes ordered according to their r_{100} values. To quantify the correlated presence or absence of genes in different lists we used a measure of mutual information (7) named here as historical mutual information (HMI) to emphasize the subjective nature of this measure because it depends on both functional relatedness of the genes and biased availability or inclusion of data (see supplementary methods and the 6_HMI_explorer.py program for exploring clusters of genes interactively). Using HMI to cluster these genes revealed three major clusters (64, 20, and 14 genes) and two other unconnected genes (Fig. 8*A*, Table S2) when communities are formed with a threshold distance (1- HMI) of 0.9 or less for a link between two genes.

Only one cluster (cluster 1 in Fig. 8*A*) had significant numbers of genes associated with gene ontology terms (Table S3). These genes encode proteins involved in RNA silencing and/or play roles in other processes such as cell division and germ cell development. Consistently, this

cluster also had the greatest number of genes that have been described in multiple publications (Fig. 8*B*), including all the genes that have been featured in abstracts on RNA silencing (Fig. 8*C*). Therefore, the analysis of additional genes in this cluster could be relevant for RNA silencing and connect it to other processes (e.g., the cell cycle). Several predicted interactions are consistent with this speculation. One, among the other genes in cluster 1 is the gene encoding PAR-5, which is predicted to selectively interact with the known regulator of RNA silencing PID-2 (Fig. 7). The predicted interaction could have a role in segregating PID-2, and potentially other components of Z-granules, to the posterior side before the first cell division during embryonic development (58). Two, cluster 1 also includes the gene encoding MCM-7, which is predicted to selectively interact with CSR-1 (ranking score 0.59 in Fig. 8*F*; also see Fig. S7 and Movie S80). This interaction is also supported by an immunoprecipitation experiment (54) and it could have a role in the chromosome segregation function of CSR-1 (65) because of the established role of the MCM complex in DNA replication (66). Three, two other proteins encoded by genes in this cluster that were also tested (CEY-2 and PAN-1) are predicted to interact with some RNA regulators (8 of 40 potential interactions tested in Fig. 8*F*; also see Fig. S7 and Movies S81 to S88).

Since six of the eight pseudogenes are in a small cluster (Fig. 8*E*, 6 of 14 genes in cluster 2), the other genes in this cluster could potentially be targets of regulation without specific downstream regulation or be co-regulated sensors of pseudogene RNA levels. Two PIRE proteins (PIRE-3/E01G4.5 and PIRE-5/K02E2.6) are also present in this cluster. Another gene Y47H10A.5 encodes a protein with similarity to decapping nuclease (Foldseek, E-value < 0.05) and is targeted by miR-243 (67), leading to RDE-1-dependent small RNA production (67,68). Since, the Y47H10A.5 protein is predicted to interact with multiple regulators of RNA silencing (Fig. 8*F*, Table S2, Fig. S7, and Movies S89 to S93), we refer to it as PIRE-9.

There is a large overlap between a set of genes that require HRDE-1 for downregulation (67 genes in both replicates from worms grown at 15ºC (69)) and genes in a single cluster (Fig. 8*F*, 20 of 64 genes in cluster 3). One possible explanation for this abundance and clustering could be that *hrde-1*-dependent gene lists are among the most numerous generated by the field and/or included in our analysis (42 of 398 lists). Alternatively, genes that are subject to HRDE-1-dependent silencing could be extensively regulated by many other regulators and require this additional downregulation for fitness – i.e., overexpression of these genes is detrimental. Consistent with this possibility, loss of HRDE-1 results in progressive sterility that can be reversed by restoring HRDE-1 activity (69). Also, as expected for the use of HRDE-1 downstream of SID-1, genes upregulated using *sid-1* (18 genes in animals lacking *sid-1* (16)) overlap with genes in the same cluster (Fig. 8*F* and Table S2, 4 of 64 in cluster 3).

In addition to these hypotheses, how interacting with PIRE proteins modulates the functions of known regulators of RNA silencing could be experimentally tested (Table S3). Future studies by labs working on multiple aspects of RNA silencing in *C. elegans* have the potential to test and enrich the classification of the regulated yet understudied genes revealed here, including by identifying many more PIRE proteins.

Discussion

Our analysis has identified selectively regulated yet understudied genes in the field of RNA silencing in *C. elegans*, some of which encode predicted influencers of RNA-regulated expression that act through protein-protein interactions. To facilitate easy inspection of all the predicted interactions identified in this study, we generated a network diagram (Fig. 8*G*) that summarizes the 77 predicted interactions among 42 interactors with varying amounts of support. Minimally, all interactions shown are predicted by AlphaFold 2.3. A survey of the information available on WormBase for all 42 interactors revealed that 8 of these interactions are already supported by some experimental evidence for physical interaction. We note that this is not an exhaustive list of

all possible interactions even among the 42 interactors considered and expect that future experimental work will refine this view.

The inevitable bias of progress. Bias during progress in a field is unavoidable and its causes are complex, including availability of technology, researcher pre-disposition, perceived importance of a direction, current societal need, etc. Therefore, the comprehensive appraisal of a field through equal representation of all important aspects is impractical. Indeed, our analysis involved the manual collation of many datasets for comparison, which could have resulted in omissions and inclusions that spark disagreements. While future extensions of this work could automate the process of aggregating and comparing data, flexible inclusion of different lists in the analysis would be needed to enable customization based on the expertise, interests, and risk tolerance of individual labs. Furthermore, earlier studies using older technologies could have led to conclusions that need revision. For example, when analyzed using multi-copy transgenes, the dsRNA-binding protein RDE-4 showed a cell non-autonomous effect (70,71), but when analyzed using single-copy transgenes, RDE-4 showed a cell autonomous effect (72). Since different researchers could interpret such conflicting data differently (e.g., differences in levels of tissue-restricted expression versus differences in extent of misexpression in other tissues), it is useful to preserve the ability to customize lists. With the expanding number of lists generated by large-scale experimental approaches in different fields, identifying selectively regulated yet understudied genes could aid the prioritization of genes for detailed mechanistic studies using the limited resources and time available for any lab.

Function(s) of the x-dependent gene. Different properties of a single protein or RNA could be important for different biological roles (73,74), or the same properties could be important for different processes. Despite such variety, a gene found in many lists could become associated with a single label because of the historical sequence of discovery (e.g., HRDE-1-dependent genes; many in cluster 3, Fig. 8*E*), thereby obscuring additional roles of that gene. Most of the PIRE proteins are predicted to interact with more than one tested regulator of RNA silencing (e.g., ten in Fig. S3). If these interactions are validated through experimental analyses, it will not be possible to classify these PIRE proteins into single pathways. Indeed it can be challenging to delineate pathways when multiple regulators in an intersecting network make quantitative contributions to an observed effect (20). The well-recognized difficulty in defining the function of a gene (75) is exacerbated in these cases, making it more appropriate to consider these proteins as entities within a system whose roles depend on context (see (76) for similar ideas).

Metrics for historically contingent progress. Exhaustive collation of past progress can be difficult because of the many formats in which data and inferences are presented. Of these, tabular data are particularly amenable to future computation. The simple r_g metric provides a weighted sum of frequently occurring features (e.g., genes) for prioritizing the top 25 genes (Fig. 1) or 100 genes (Fig. 8). However, the number of genes considered for calculating r_g can influence the prioritized set obtained (Table S4). Specifically, the same genes were identified as the top 25 genes by considering 1000 genes (1000th r_{1000} gene being present in 53 lists) or 100 genes (100th r_{100} gene being present in 72 lists), and 16 of these genes were identified by considering 25 genes (25th r_{25} gene being present in 84 lists). More complicated metrics that consider other useful aspects of the data such as effect size (77) of the reported change (e.g., measured for fold-change when using RNA-seq), discoverability of the change using a technique (e.g., influenced by abundance of a protein for immunoprecipitation), and reliability of the technique used (e.g., adequacy of replicates for estimating noise) could be developed in the future to extract more information. Historical mutual information provides a measure of predictability that is an unknown mix of functional relatedness and biased attention, hence 'historical'. This metric is simply a normalized measure of mutual information (78), which captures the predictability of one feature given knowledge about another feature and is widely used (79) because of the ability to capture

both correlations and anticorrelations without any knowledge of underlying causality. The tendency to progress by building upon past discoveries and to communicate by connecting to concepts of perceived importance makes the growth of knowledge akin to growth of networks through preferential attachment (see simulation in Movie S94). Metrics that take advantage of this aspect could be developed to reduce bias in the information (e.g., by weighting based on community size). However, separating features that appear to be important based on progress in a field from what is inherently important given the characteristics of a system can be challenging.

From transcript changes to protein-protein interactions. Positive feedback loops that drive growth and development are a ubiquitous feature of life (80). Yet, living systems are also characterized by homeostasis (4), which needs negative feedback to suppress runaway processes. For example, in a chain of biochemical reactions, product inhibition (81) can be used to regulate production to match need. While this organization enables compensation in response to change, complete compensation for all processes is clearly not possible as evidenced by the fact that many mutations have measurable consequences. A specific case of this general principle is transcriptional adaptation, where the mutation-induced degradation of a transcript results in compensatory changes in the levels of other transcripts (82). The existence of PIRE proteins suggests that another way for organisms to compensate for the perturbation of a protein that regulates a process is to change the levels of other proteins that can regulate the same process through protein-protein interactions. Thus, we speculate that perturbing a protein could sometimes alter the mRNA levels of its interactors because of the prevalence of feedback regulation in living systems. If true, this feature of life provides a strategy for combining RNA sequencing and protein structure predictions to identify protein-protein interactions of regulatory importance.

Data Availability

All scripts used in this study are available at GitHub (AntonyJose-Lab/Lalit_Jose_2024) and has been archived at Zenodo (https://zenodo.org/records/13952718).

Funding

This work is supported in part by National Institutes of Health Grant R01GM124356 and National Science Foundation Grant 2120895 to A.M.J.

Acknowledgements

We thank Tom Kocher, Brian Pierce, and members of the Jose lab for comments on the manuscript; four anonymous reviewers for their feedback and suggestions; Brian Pierce for discussions and Rui Yin for installing AlphaFold 2 on the UMD HPCC; and Carlos Retamal and José Feijo for getting us started with AlphaFold. We acknowledge the University of Maryland supercomputing resources (http://hpcc.umd.edu) made available for conducting the research reported in this paper.

References

1. Jose, A.M. (2020) The analysis of living systems can generate both knowledge and illusions. *Elife*, **9**, e56354.
2. Richardson, R.A.K., Navarro, H.T., Nunes Amaral, L.A. and Stoeger, T. (2023) Meta-Research: understudied genes are lost in a leaky pipeline between genome-wide assays and reporting of results. *eLife*, **12**, RP93429.
3. Rocha, J.J., Jayaram, S.A., Stevens, T.J., Muschalik, N., Shah, R.D., Emran, S., Robles, C., Freeman, M. and Munro, S. (2023) Functional unknomics: Systematic screening of conserved genes of unknown function. *PLoS Biol*, **21**, e3002222.
4. Billman, G.E. (2020) Homeostasis: The Underappreciated and Far Too Often Ignored Central Organizing Principle of Physiology. *Front Physiol*, **11**, 200.
5. Davis, P., Zarowiecki, M., Arnaboldi, V., Becerra, A., Cain, S., Chan, J., Chen, W.J., Cho, J., da Veiga Beltrame, E., Diamantakis, S. *et al.* (2022) WormBase in 2022-data, processes, and tools for analyzing Caenorhabditis elegans. *Genetics*, **220**, iyac003.
6. Jaccard, P. (1901) Distribution de la flore alpine dans le bassin des dranses et dans quelques régions voisines. *Bulletin de la Société vaudoise des sciences naturelles*, **37**, 241-272.
7. Witten, I.H. and Frank, E. (2005) *Data Mining: Practical Machine Learning Tools and Techniques*. 2nd ed. Morgan Kaufmann, San Francisco.
8. Girvan, M. and Newman, M.E. (2002) Community structure in social and biological networks. *Proc Natl Acad Sci U S A*, **99**, 7821-7826.
9. Ashburner, M., Ball, C.A., Blake, J.A., Botstein, D., Butler, H., Cherry, J.M., Davis, A.P., Dolinski, K., Dwight, S.S., Eppig, J.T. *et al.* (2000) Gene ontology: tool for the unification of biology. The Gene Ontology Consortium. *Nat Genet*, **25**, 25-29.
10. Consortium, G.O., Aleksander, S.A., Balhoff, J., Carbon, S., Cherry, J.M., Drabkin, H.J., Ebert, D., Feuermann, M., Gaudet, P., Harris, N.L. *et al.* (2023) The Gene Ontology knowledgebase in 2023. *Genetics*, **224**.
11. Evans, R., O'Neill, M., Pritzel, A., Antropova, N., Senior, A., Green, T., Žídek, A., Bates, R., Blackwell, S., Yim, J. *et al.* (2022) Protein complex prediction with AlphaFold-Multimer. *bioRxiv*, 2021.2010.2004.463034.
12. Jumper, J., Evans, R., Pritzel, A., Green, T., Figurnov, M., Ronneberger, O., Tunyasuvunakool, K., Bates, R., Zidek, A., Potapenko, A. *et al.* (2021) Highly accurate protein structure prediction with AlphaFold. *Nature*, **596**, 583-589.
13. Abramson, J., Adler, J., Dunger, J., Evans, R., Green, T., Pritzel, A., Ronneberger, O., Willmore, L., Ballard, A.J., Bambrick, J. *et al.* (2024) Accurate structure prediction of biomolecular interactions with AlphaFold 3. *Nature*, **630**, 493–500.
14. Meng, E.C., Goddard, T.D., Pettersen, E.F., Couch, G.S., Pearson, Z.J., Morris, J.H. and Ferrin, T.E. (2023) UCSF ChimeraX: Tools for structure building and analysis. *Protein Sci*, **32**, e4792.
15. Buckley, B.A., Burkhart, K.B., Gu, S.G., Spracklin, G., Kershner, A., Fritz, H., Kimble, J., Fire, A. and Kennedy, S. (2012) A nuclear Argonaute promotes multigenerational epigenetic inheritance and germline immortality. *Nature*, **489**, 447-451.

16. Shugarts, N., Sathya, A., Yi, A.L., Chan, W.M., Marré, J.A. and Jose, A.M. (2024) Intergenerational transport of double-stranded RNA limits heritable epigenetic changes. *eLife*.
17. van Kempen, M., Kim, S.S., Tumescheit, C., Mirdita, M., Lee, J., Gilchrist, C.L.M., Soding, J. and Steinegger, M. (2024) Fast and accurate protein structure search with Foldseek. *Nat Biotechnol*, **42**, 243-246.
18. Fischer, S.E.J. and Ruvkun, G. (2020) Caenorhabditis elegans ADAR editing and the ERI-6/7/MOV10 RNAi pathway silence endogenous viral elements and LTR retrotransposons. *Proc Natl Acad Sci U S A*, **117**, 5987-5996.
19. Devanapally, S., Raman, P., Chey, M., Allgood, S., Ettefa, F., Diop, M., Lin, Y., Cho, Y.E. and Jose, A.M. (2021) Mating can initiate stable RNA silencing that overcomes epigenetic recovery. *Nat Commun*, **12**, 4239.
20. Knudsen-Palmer, D.R., Raman, P., Ettefa, F., De Ravin, L. and Jose, A.M. (2024) Target-specific requirements for RNA interference can arise through restricted RNA amplification despite the lack of specialized pathways. *Elife*, **13**, RP97487.
21. Perales, R., Pagano, D., Wan, G., Fields, B.D., Saltzman, A.L. and Kennedy, S.G. (2018) Transgenerational Epigenetic Inheritance Is Negatively Regulated by the HERI-1 Chromodomain Protein. *Genetics*, **210**, 1287-1299.
22. Rogers, A.K. and Phillips, C.M. (2020) A Small-RNA-Mediated Feedback Loop Maintains Proper Levels of 22G-RNAs in C. elegans. *Cell Rep*, **33**, 108279.
23. Frolows, N. and Ashe, A. (2021) Small RNAs and chromatin in the multigenerational epigenetic landscape of Caenorhabditis elegans. *Philos Trans R Soc Lond B Biol Sci*, **376**, 20200112.
24. Billi, A.C., Fischer, S.E. and Kim, J.K. (2014) Endogenous RNAi pathways in C. elegans. *WormBook*, 1-49.
25. Sundby, A.E., Molnar, R.I. and Claycomb, J.M. (2021) Connecting the Dots: Linking Caenorhabditis elegans Small RNA Pathways and Germ Granules. *Trends Cell Biol*, **31**, 387-401.
26. Yin, R., Feng, B.Y., Varshney, A. and Pierce, B.G. (2022) Benchmarking AlphaFold for protein complex modeling reveals accuracy determinants. *Protein Sci*, **31**, e4379.
27. Bryant, P., Pozzati, G. and Elofsson, A. (2022) Improved prediction of protein-protein interactions using AlphaFold2. *Nat Commun*, **13**, 1265.
28. Herschlag, D. and Pinney, M.M. (2018) Hydrogen Bonds: Simple after All? *Biochemistry*, **57**, 3338-3352.
29. Humphreys, I.R., Pei, J., Baek, M., Krishnakumar, A., Anishchenko, I., Ovchinnikov, S., Zhang, J., Ness, T.J., Banjade, S., Bagde, S.R. *et al.* (2021) Computed structures of core eukaryotic protein complexes. *Science*, **374**, eabm4805.
30. Weeratunga, S., Gormal, R.S., Liu, M., Eldershaw, D., Livingstone, E.K., Malapaka, A., Wallis, T.P., Bademosi, A.T., Jiang, A., Healy, M.D. *et al.* (2024) Interrogation and validation of the interactome of neuronal Munc18-interacting Mint proteins with AlphaFold2. *J Biol Chem*, **300**, 105541.
31. Harper, J.W. and Schulman, B.A. (2021) Cullin-RING Ubiquitin Ligase Regulatory Circuits: A Quarter Century Beyond the F-Box Hypothesis. *Annu Rev Biochem*, **90**, 403-429.

32. Dearlove, E.L., Chatrin, C., Buetow, L., Ahmed, S.F., Schmidt, T., Bushell, M., Smith, B.O. and Huang, D.T. (2024) DTX3L ubiquitin ligase ubiquitinates single-stranded nucleic acids. *Elife*, **13**.
33. Shi, C.Y., Kingston, E.R., Kleaveland, B., Lin, D.H., Stubna, M.W. and Bartel, D.P. (2020) The ZSWIM8 ubiquitin ligase mediates target-directed microRNA degradation. *Science*, **370**.
34. Han, J., LaVigne, C.A., Jones, B.T., Zhang, H., Gillett, F. and Mendell, J.T. (2020) A ubiquitin ligase mediates target-directed microRNA decay independently of tailing and trimming. *Science*, **370**.
35. Gudipati, R.K., Braun, K., Gypas, F., Hess, D., Schreier, J., Carl, S.H., Ketting, R.F. and Grosshans, H. (2021) Protease-mediated processing of Argonaute proteins controls small RNA association. *Mol Cell*, **81**, 2388-2402.
36. Placentino, M., de Jesus Domingues, A.M., Schreier, J., Dietz, S., Hellmann, S., de Albuquerque, B.F., Butter, F. and Ketting, R.F. (2021) Intrinsically disordered protein PID-2 modulates Z granules and is required for heritable piRNA-induced silencing in the Caenorhabditis elegans embryo. *EMBO J*, **40**, e105280.
37. Wallner, B. (2023) AFsample: improving multimer prediction with AlphaFold using massive sampling. *Bioinformatics*, **39**, btad573.
38. Alderson, T.R., Pritisanac, I., Kolaric, D., Moses, A.M. and Forman-Kay, J.D. (2023) Systematic identification of conditionally folded intrinsically disordered regions by AlphaFold2. *Proc Natl Acad Sci U S A*, **120**, e2304302120.
39. Bret, H., Gao, J., Zea, D.J., Andreani, J. and Guerois, R. (2024) From interaction networks to interfaces, scanning intrinsically disordered regions using AlphaFold2. *Nat Commun*, **15**, 597.
40. Wayment-Steele, H.K., Ojoawo, A., Otten, R., Apitz, J.M., Pitsawong, W., Homberger, M., Ovchinnikov, S., Colwell, L. and Kern, D. (2024) Predicting multiple conformations via sequence clustering and AlphaFold2. *Nature*, **625**, 832-839.
41. Shor, B. and Schneidman-Duhovny, D. (2024) CombFold: predicting structures of large protein assemblies using a combinatorial assembly algorithm and AlphaFold2. *Nat Methods*, **21**, 477-487.
42. Humphreys, I.R., Zhang, J., Baek, M., Wang, Y., Krishnakumar, A., Pei, J., Anishchenko, I., Tower, C.A., Jackson, B.A., Warrier, T. *et al.* (2024) Protein interactions in human pathogens revealed through deep learning. *Nat Microbiol*, **9**, 2642-2652.
43. Yu, D., Chojnowski, G., Rosenthal, M. and Kosinski, J. (2023) AlphaPulldown-a python package for protein-protein interaction screens using AlphaFold-Multimer. *Bioinformatics*, **39**, btac749.
44. Lee, R.C., Hammell, C.M. and Ambros, V. (2006) Interacting endogenous and exogenous RNAi pathways in Caenorhabditis elegans. *RNA*, **12**, 589-597.
45. Shukla, A., Yan, J., Pagano, D.J., Dodson, A.E., Fei, Y., Gorham, J., Seidman, J.G., Wickens, M. and Kennedy, S. (2020) poly(UG)-tailed RNAs in genome protection and epigenetic inheritance. *Nature*, **582**, 283-288.
46. Park, M.C., Park, D., Lee, E.K., Park, T. and Lee, J. (2010) Genomic analysis of the telomeric length effect on organismic lifespan in Caenorhabditis elegans. *Biochem Biophys Res Commun*, **396**, 382-387.

47. LeGendre, J.B., Campbell, Z.T., Kroll-Conner, P., Anderson, P., Kimble, J. and Wickens, M. (2013) RNA targets and specificity of Staufen, a double-stranded RNA-binding protein in Caenorhabditis elegans. *J Biol Chem*, **288**, 2532-2545.
48. Alliance of Genome Resources, C. (2024) Updates to the Alliance of Genome Resources central infrastructure. *Genetics*, **227**, iyae049.
49. Chen, C.C., Simard, M.J., Tabara, H., Brownell, D.R., McCollough, J.A. and Mello, C.C. (2005) A member of the polymerase beta nucleotidyltransferase superfamily is required for RNA interference in C. elegans. *Curr Biol*, **15**, 378-383.
50. Preston, M.A., Porter, D.F., Chen, F., Buter, N., Lapointe, C.P., Keles, S., Kimble, J. and Wickens, M. (2019) Unbiased screen of RNA tailing activities reveals a poly(UG) polymerase. *Nat Methods*, **16**, 437-445.
51. Phillips, C.M., Montgomery, T.A., Breen, P.C. and Ruvkun, G. (2012) MUT-16 promotes formation of perinuclear mutator foci required for RNA silencing in the C. elegans germline. *Genes Dev*, **26**, 1433-1444.
52. Uebel, C.J., Anderson, D.C., Mandarino, L.M., Manage, K.I., Aynaszyan, S. and Phillips, C.M. (2018) Distinct regions of the intrinsically disordered protein MUT-16 mediate assembly of a small RNA amplification complex and promote phase separation of Mutator foci. *PLoS Genet*, **14**, e1007542.
53. Flynn, S.M., Chen, C., Artan, M., Barratt, S., Crisp, A., Nelson, G.M., Peak-Chew, S.Y., Begum, F., Skehel, M. and de Bono, M. (2020) MALT-1 mediates IL-17 neural signaling to regulate C. elegans behavior, immunity and longevity. *Nat Commun*, **11**, 2099.
54. Singh, M., Cornes, E., Li, B., Quarato, P., Bourdon, L., Dingli, F., Loew, D., Proccacia, S. and Cecere, G. (2021) Translation and codon usage regulate Argonaute slicer activity to trigger small RNA biogenesis. *Nat Commun*, **12**, 3492.
55. Tsai, H.Y., Chen, C.C., Conte, D., Jr., Moresco, J.J., Chaves, D.A., Mitani, S., Yates, J.R., 3rd, Tsai, M.D. and Mello, C.C. (2015) A ribonuclease coordinates siRNA amplification and mRNA cleavage during RNAi. *Cell*, **160**, 407-419.
56. Chey, M.S., Raman, P., Ettefa, F. and Jose, A.M. (2024) Evidence for multiple forms of heritable RNA silencing. *bioRxiv*.
57. Shah, V.N., Neumeier, J., Huberdeau, M.Q., Zeitler, D.M., Bruckmann, A., Meister, G. and Simard, M.J. (2023) Casein kinase 1 and 2 phosphorylate Argonaute proteins to regulate miRNA-mediated gene silencing. *EMBO Rep*, e57250.
58. Morton, D.G., Shakes, D.C., Nugent, S., Dichoso, D., Wang, W., Golden, A. and Kemphues, K.J. (2002) The Caenorhabditis elegans par-5 gene encodes a 14-3-3 protein required for cellular asymmetry in the early embryo. *Dev Biol*, **241**, 47-58.
59. Johnson, C., Crowther, S., Stafford, M.J., Campbell, D.G., Toth, R. and MacKintosh, C. (2010) Bioinformatic and experimental survey of 14-3-3-binding sites. *Biochem J*, **427**, 69-78.
60. Hong, Y. (2018) aPKC: the Kinase that Phosphorylates Cell Polarity. *F1000Res*, **7**, Rev-903.
61. Strittmatter, S.M., Valenzuela, D., Kennedy, T.E., Neer, E.J. and Fishman, M.C. (1990) G0 is a major growth cone protein subject to regulation by GAP-43. *Nature*, **344**, 836-841.
62. Hajdu-Cronin, Y.M., Chen, W.J., Patikoglou, G., Koelle, M.R. and Sternberg, P.W. (1999) Antagonism between G(o)alpha and G(q)alpha in Caenorhabditis elegans: the RGS protein

EAT-16 is necessary for G(o)alpha signaling and regulates G(q)alpha activity. *Genes Dev*, **13**, 1780-1793.

63. Nurrish, S., Ségalat, L. and Kaplan, J.M. (1999) Serotonin inhibition of synaptic transmission: Gαo decreases the abundance of UNC-13 at release sites. *Neuron*, **24**, 231-242.
64. Jose, A.M. and Koelle, M.R. (2005) Domains, amino acid residues, and new isoforms of Caenorhabditis elegans diacylglycerol kinase 1 (DGK-1) important for terminating diacylglycerol signaling in vivo. *J Biol Chem*, **280**, 2730-2736.
65. Claycomb, J.M., Batista, P.J., Pang, K.M., Gu, W., Vasale, J.J., van Wolfswinkel, J.C., Chaves, D.A., Shirayama, M., Mitani, S., Ketting, R.F. *et al.* (2009) The Argonaute CSR-1 and its 22G-RNA cofactors are required for holocentric chromosome segregation. *Cell*, **139**, 123-134.
66. Li, N., Zhai, Y., Zhang, Y., Li, W., Yang, M., Lei, J., Tye, B.K. and Gao, N. (2015) Structure of the eukaryotic MCM complex at 3.8 A. *Nature*, **524**, 186-191.
67. Correa, R.L., Steiner, F.A., Berezikov, E. and Ketting, R.F. (2010) MicroRNA-directed siRNA biogenesis in Caenorhabditis elegans. *PLoS Genet*, **6**, e1000903.
68. Gu, W., Shirayama, M., Conte, D., Jr., Vasale, J., Batista, P.J., Claycomb, J.M., Moresco, J.J., Youngman, E.M., Keys, J., Stoltz, M.J. *et al.* (2009) Distinct argonaute-mediated 22G-RNA pathways direct genome surveillance in the C. elegans germline. *Mol Cell*, **36**, 231-244.
69. Ni, J.Z., Kalinava, N., Chen, E., Huang, A., Trinh, T. and Gu, S.G. (2016) A transgenerational role of the germline nuclear RNAi pathway in repressing heat stress-induced transcriptional activation in *C. elegans*. *Epigenetics Chromatin*, **9**, 3.
70. Jose, A.M., Garcia, G.A. and Hunter, C.P. (2011) Two classes of silencing RNAs move between Caenorhabditis elegans tissues. *Nat Struct Mol Biol*, **18**, 1184-1188.
71. Blanchard, D., Parameswaran, P., Lopez-Molina, J., Gent, J., Saynuk, J.F. and Fire, A. (2011) On the nature of in vivo requirements for rde-4 in RNAi and developmental pathways in C. elegans. *RNA Biol*, **8**, 458-467.
72. Raman, P., Zaghab, S.M., Traver, E.C. and Jose, A.M. (2017) The double-stranded RNA binding protein RDE-4 can act cell autonomously during feeding RNAi in C. elegans. *Nucleic Acids Res*, **45**, 8463-8473.
73. Chapple, C.E., Robisson, B., Spinelli, L., Guien, C., Becker, E. and Brun, C. (2015) Extreme multifunctional proteins identified from a human protein interaction network. *Nat Commun*, **6**, 7412.
74. Ribeiro, D.M., Briere, G., Bely, B., Spinelli, L. and Brun, C. (2019) MoonDB 2.0: an updated database of extreme multifunctional and moonlighting proteins. *Nucleic Acids Res*, **47**, D398-D402.
75. Keeling, D.M., Garza, P., Nartey, C.M. and Carvunis, A.R. (2019) The meanings of 'function' in biology and the problematic case of de novo gene emergence. *Elife*, **8**, e47014.
76. Kwon, J.J., Pan, J., Gonzalez, G., Hahn, W.C. and Zitnik, M. (2024) On knowing a gene: A distributional hypothesis of gene function. *Cell Systems*, **15**, 488-496.
77. Lakens, D. (2013) Calculating and reporting effect sizes to facilitate cumulative science: a practical primer for t-tests and ANOVAs. *Front Psychol*, **4**, 863.
78. Cover, T.M. and Thomas, J.A. (2006) *Elements of Information Theory (Wiley Series in Telecommunications and Signal Processing)*. Wiley-Interscience.

79. Uda, S. (2020) Application of information theory in systems biology. *Biophys Rev*, **12**, 377-384.
80. Jose, A.M. (2024) Heritable epigenetic changes are constrained by the dynamics of regulatory architectures. *eLife*, **12**, RP92093.
81. Frieden, E. and Walter, C. (1963) Prevalence and Significance of the Product Inhibition of Enzymes. *Nature*, **198**, 834-837.
82. Sztal, T.E. and Stainier, D.Y.R. (2020) Transcriptional adaptation: a mechanism underlying genetic robustness. *Development*, **147**, dev186452.
83. Varadi, M., Anyango, S., Deshpande, M., Nair, S., Natassia, C., Yordanova, G., Yuan, D., Stroe, O., Wood, G., Laydon, A. *et al.* (2022) AlphaFold Protein Structure Database: massively expanding the structural coverage of protein-sequence space with high-accuracy models. *Nucleic Acids Res*, **50**, D439-D444.

Figures and Figure Legends

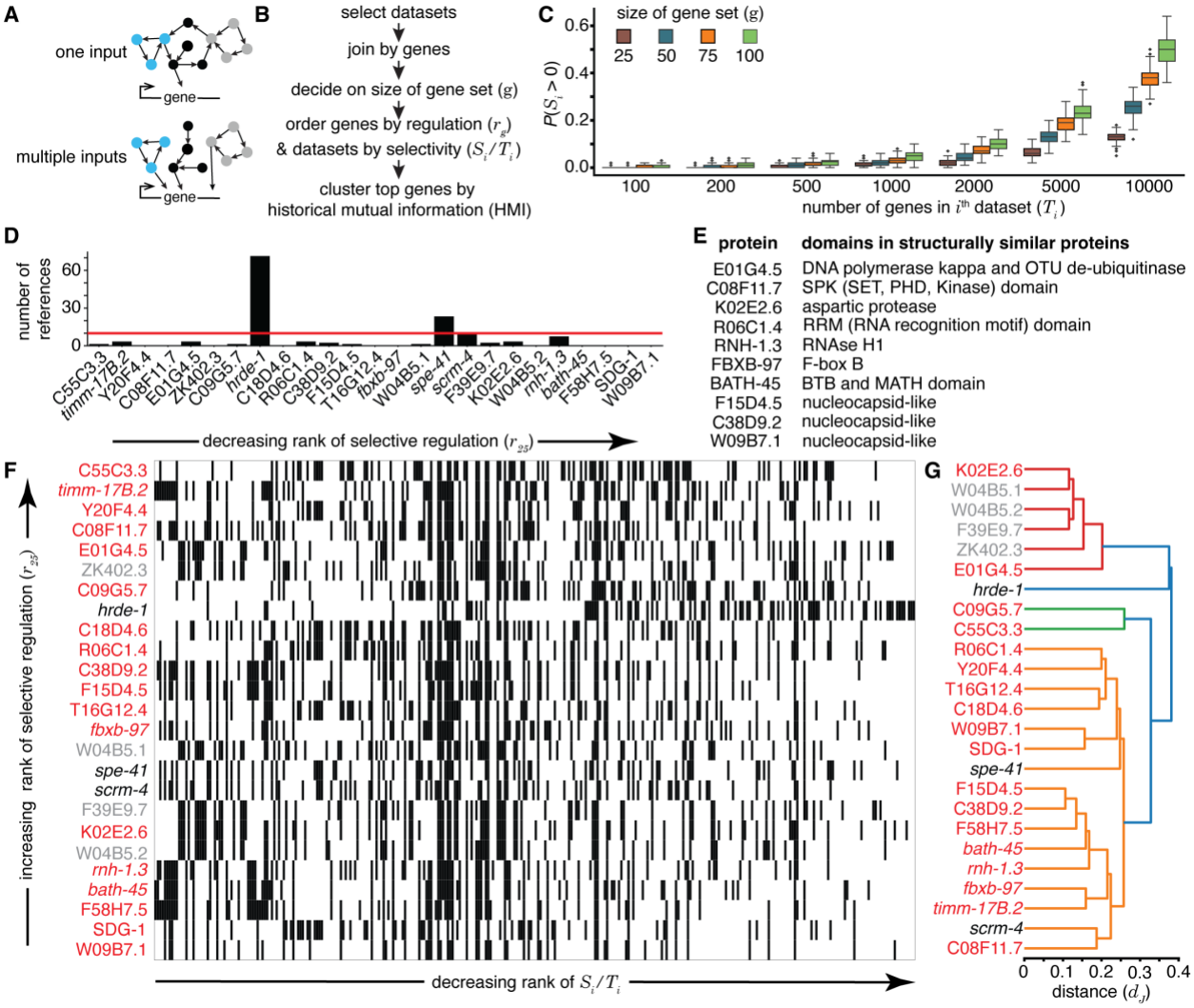

Figure 1. Some genes are selectively regulated, reported as part of many lists, and yet are understudied. (*A*) Schematics of possible regulatory architectures for genes found on multiple lists. (*top*) Gene receiving one input form a large network. (*bottom*) Gene receiving multiple inputs from separable networks. (*B*) Strategy for the identification of regulated genes. See Methods for details. (*C*) Relationship between S_i, T_i, and g obtained using simulated data for an organism with 20,000 genes. Distributions of the probabilities of having at least one overlapping gene within the selected gene set ($P(S_i > 0)$) for 100 runs of each parameter combination are presented as box and whisker plots. (*D*) Numbers of publications listed on WormBase for the top 25 regulated genes ordered using r_{25} in the field of RNA silencing in *C. elegans*. Red line marks 10 publications. (*E*) Domains present in proteins encoded by understudied genes among the top 25 genes that are suggestive of function. Proteins with high-confidence AlphaFold structures (12) were used to identify similar proteins as detected by Foldseek (17) or based on the literature ((18); C38D9.2, F15D4.5, and W09B7.2). (*F*) Heatmap showing the top 25 regulated genes. Presence (black) or absence (white) of each gene in each dataset is indicated. Relatively understudied (<10 references on WormBase) genes (red) or pseudogenes (grey) identified in (*D*) are indicated. (*G*) Hierarchical clustering of the top 25 genes based on co-occurrence in lists, where gene names colored as in (*F*) and 'distance (d_J)' indicates Jaccard distance.

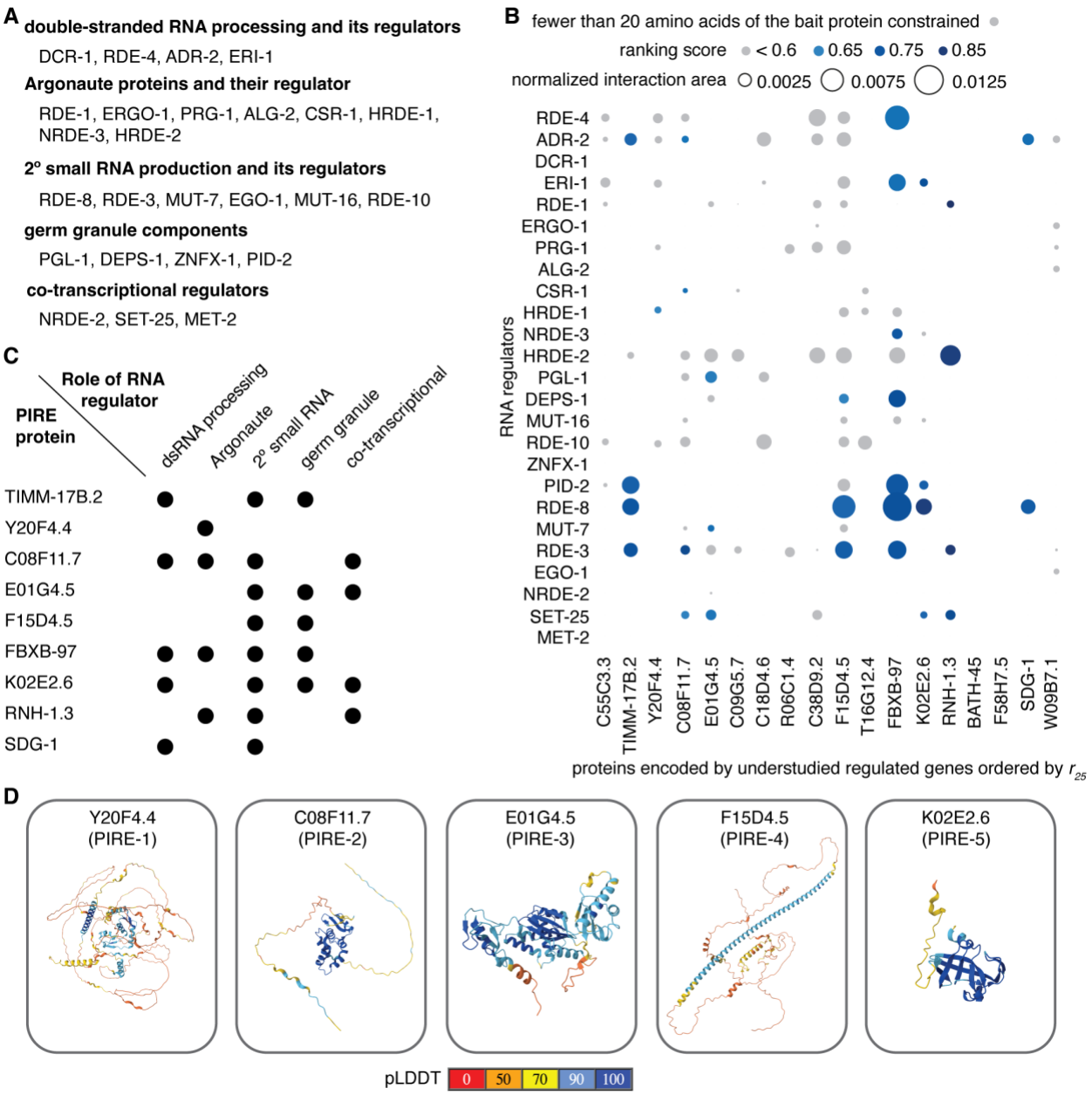

Figure 2. Understudied regulated genes encode proteins predicted to interact with key regulators of RNA silencing. (*A*) Regulators of RNA silencing in different categories examined for predicted interactions with proteins encoded by understudied genes identified in this study. See text for details. (*B*) Predicted interactions between proteins encoded by top 25 genes ordered by their r_{25} scores and known regulators of RNA silencing in *C. elegans*. The area of the interaction surface between partners normalized by the product of the sizes of the interactors is shown as a bubble plot (inter-protein predicted aligned error <5Å and inter-residue distance <6Å). Interactions with a low ranking score (< 0.6) and/or that constrain fewer that 20 amino acids in proteins encoded by the understudied genes are indicated in grey. Also see Fig. S1 and Movies S1 to S32. (*C*) Proteins encoded by understudied genes with significant interactions are predicted to impact multiple steps in RNA silencing. (*D*) Predicted structures for the five newly named predicted influencers of RNA-regulated expression (PIRE) proteins are shown with the per-residue confidence (pLDDT) as present in the AlphaFold protein database (83).

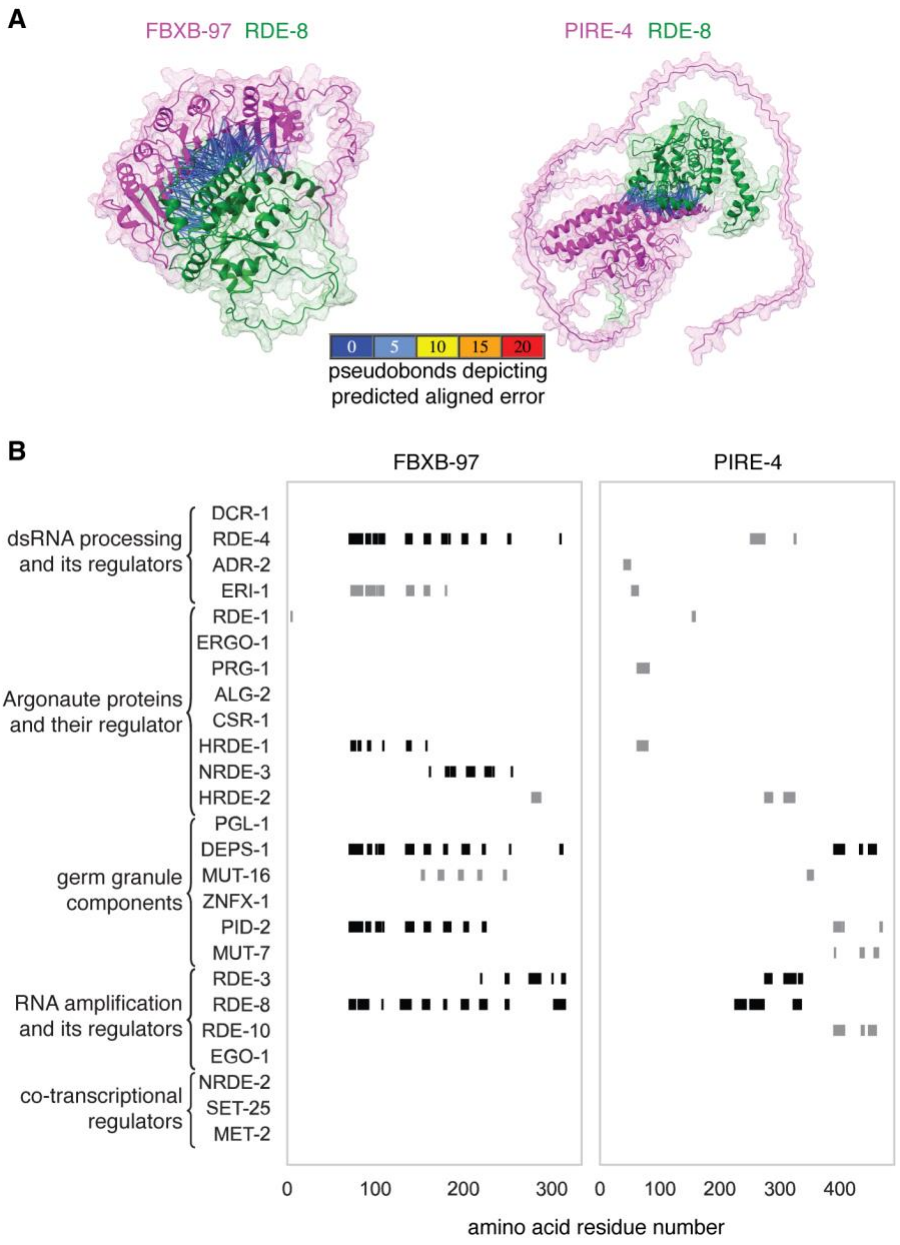

Figure 3. Predicted Influencer of RNA-regulated Expression (PIRE) proteins interact with regulators of RNA silencing in two general modes. (*A*) Predicted interactions between the PIRE proteins (magenta) FBXB-97 (left) and PIRE-3 (right) with the known regulator RDE-8 (green) that are of high confidence (constraining more than 20 amino acid residues with an inter-Cα distance less than 6Å and PAE less than 5Å) are indicated with pseudo bonds. (*B*) Regions of the PIRE protein sequence constrained by the interacting regulator. Markers (black, ranking score >0.6; grey, ranking score <0.6) are enlarged with respect to the X-axis for visibility (e.g., the marker denoting the interaction between RDE-1 and FBXB-97 only indicates one residue).

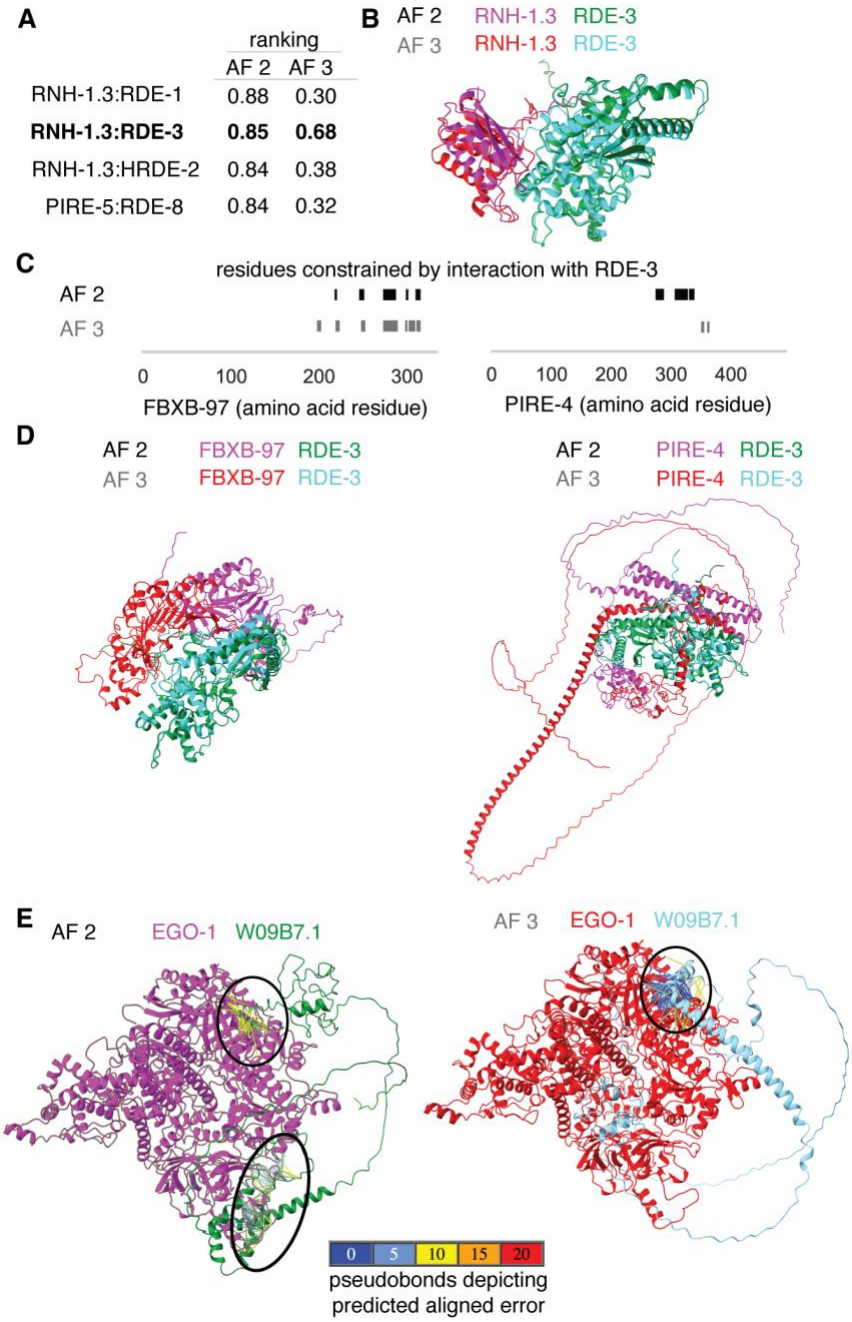

Figure 4. Interactions predicted by AlphaFold 2 and by the AlphaFold 3 server can differ. (*A*) Comparison of the top ranking interactions between known regulators of RNA silencing and the PIRE proteins predicted by AlphaFold 2 (AF 2 (11); 0.8*ipTM + 0.2*pTM) with the score generated by AlphaFold 3 (AF3 (13); 0.8*ipTM + 0.2*pTM + 0.5*disorder). A high-confidence prediction by both approaches is highlighted in bold. (*B*) Models for the interaction of RNH-1.3 with RDE-3 generated by AF2 and AF3 overlayed using RDE-3. Also see Movie S33. (*C*) Comparison of residues of PIRE proteins constrained through interactions as predicted by AF2 (black) or by AF3 (grey). (*D*) Comparison of interactions between FBXB-97 and RDE-3 (left), and between PIRE-4 and RDE-3 (right) as predicted by AF2 (black) and the AF3 server (grey), respectively. Structures are shown with differential coloring of each protein and overlayed using the RDE-3 structures in both cases. Also see Movies S34 and S35. (*E*) Interactions between

EGO-1 (magenta or red) and W09B7.1 (green or cyan) predicted by AF2 or AF3. Black ovals indicate interacting regions with inter-protein PAE <10Å (left) or <5Å (right). Also see Movie S36.

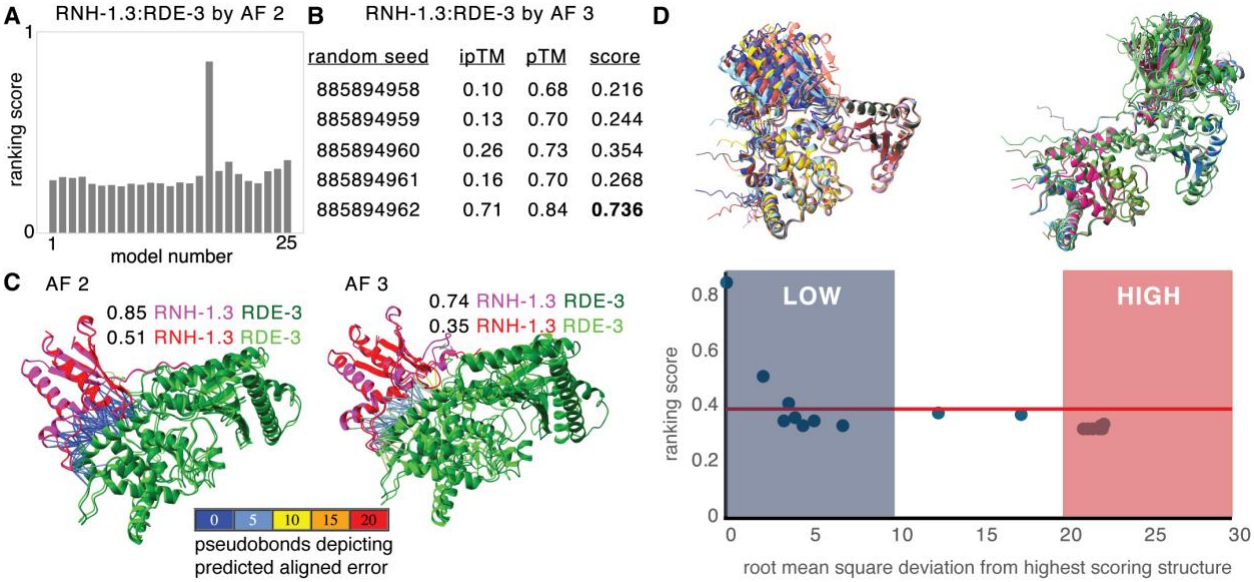

Figure 5. High-ranking models can be rare, and models can converge early with increasing scores. (*A*) Distribution of ranking scores for the 25 models of RNH-1.3:RDE-3 generated by AF 2. (*B*) Multiple runs with different random seeds and resulting scores for models of RNH-1.3:RDE-3 generated by AF 3. (*C*) Overlay of models with the highest scores from two different runs showing similar interactions between RNH-1.3 (magenta or red) and RDE-3 (green or lime) predicted by both AF 2 and AF 3. Pseudobonds depicting the predicted aligned errors for the constrained residues are highlighted for both pairs of models. Also see Movie S37 and S38. (*D*) A range of scores can underlie nearly similar architectures of a predicted complex. The highest scoring model for RNH-1.3:RDE-3 from each of 18 AF 2 runs (different colors) were superimposed using RDE-3. *Top*, Superimposed models for low (less than 10Å) and high (more than 20Å) root mean square deviation (RMSD) values are shown. *Bottom*, Ranking scores are plotted after arranging models in increasing order of RMSD from the highest scoring model.

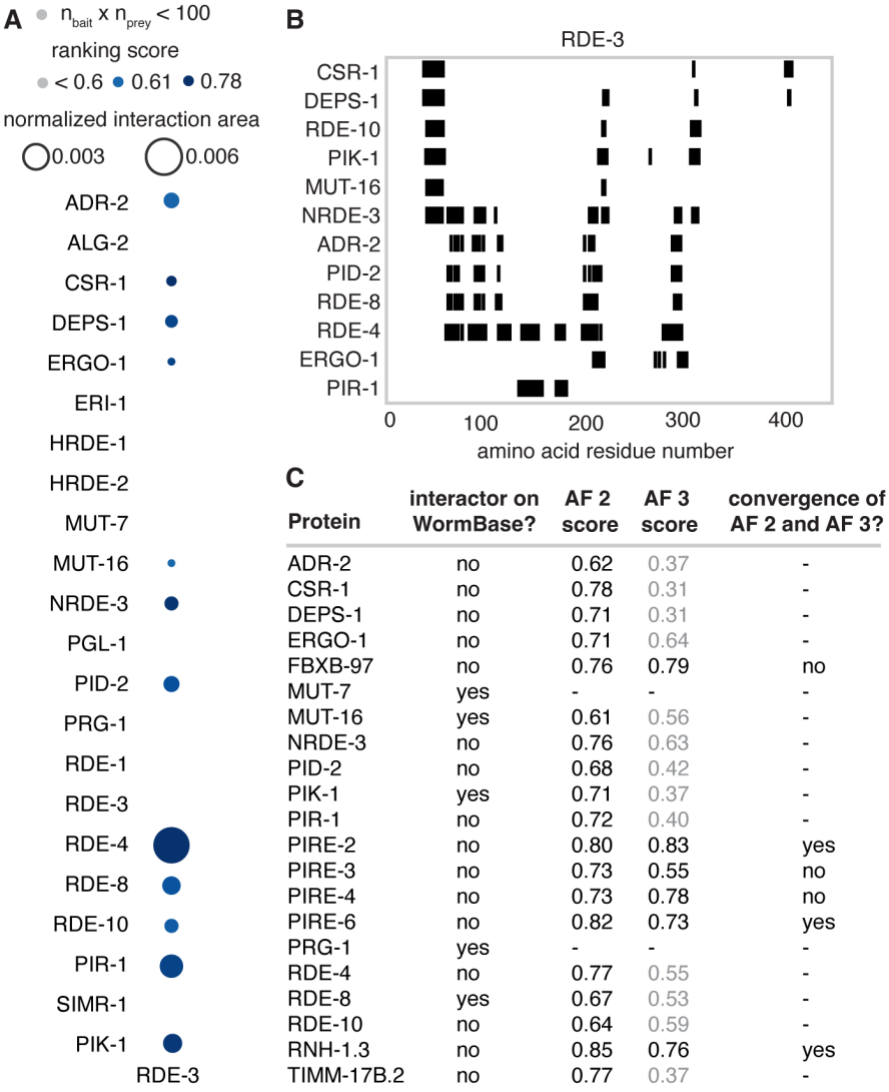

C

Protein	interactor on WormBase?	AF 2 score	AF 3 score	convergence of AF 2 and AF 3?
ADR-2	no	0.62	0.37	-
CSR-1	no	0.78	0.31	-
DEPS-1	no	0.71	0.31	-
ERGO-1	no	0.71	0.64	-
FBXB-97	no	0.76	0.79	no
MUT-7	yes	-	-	-
MUT-16	yes	0.61	0.56	-
NRDE-3	no	0.76	0.63	-
PID-2	no	0.68	0.42	-
PIK-1	yes	0.71	0.37	-
PIR-1	no	0.72	0.40	-
PIRE-2	no	0.80	0.83	yes
PIRE-3	no	0.73	0.55	no
PIRE-4	no	0.73	0.78	no
PIRE-6	no	0.82	0.73	yes
PRG-1	yes	-	-	-
RDE-4	no	0.77	0.55	-
RDE-8	yes	0.67	0.53	-
RDE-10	no	0.64	0.59	-
RNH-1.3	no	0.85	0.76	yes
TIMM-17B.2	no	0.77	0.37	-

Figure 6. The poly-UG polymerase RDE-3 is predicted to interact with multiple proteins. (*A*) Predicted interactions of RDE-3 with known regulators of RNA silencing and the 5 proteins listed as physical interactors on WormBase (MUT-16, MUT-7, PIK-1, RDE-8, and PRG-1) identified by AlphaFold 2.3 are shown. Sizes of circles indicate normalized interaction area and shading indicates ranking score. Grey indicates ranking scores < 0.6 and/or the products of numbers of constrained residues in RDE-3 and its interactors (n_{bait} x n_{prey}) < 100. Also see Movies S61 to S72. (*B*) Regions of RDE-3 protein sequence constrained by the interacting regulators. Markers (black) are as in Fig. 3*B*. (*C*) Table summarizing interactors of RDE-3. Experimentally identified physical interactors (interactor on WormBase?), highest score of AF 2 predicted interactions that are > 0.6 (25 models from 1 run), highest score among AF 3 predicted interactions (25 models from 5 runs), and whether the AF 2 and AF 3 structures are similar (convergence of AF 2 and AF 3?) are indicated. Scores of AF 3 models that lack any interactions between the two proteins with a predicted aligned error < 5Å and a distance < 6Å are indicated in grey.

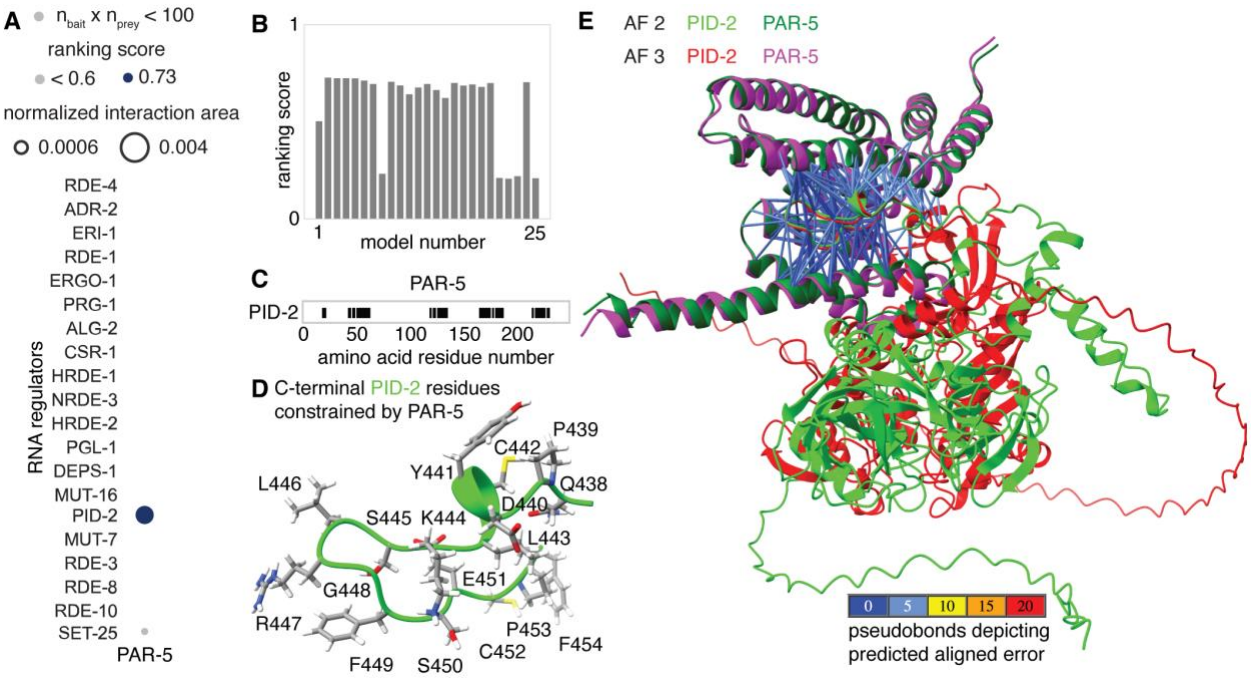

Figure 7. PAR-5 is predicted to interact with the Z-granule surface protein PID-2/ZSP-1 but not with many other tested regulators of RNA silencing. (*A*) Predicted interactions of PAR-5 with known regulators of RNA silencing identified by AlphaFold 2.3 are shown. Area of circles and shading are as in Fig. 6*A*. (*B*) Distribution of ranking scores for the 25 models of PAR-5:PID-2 generated by AF 2. (*C*) Regions of PAR-5 protein sequence constrained by interactions with PID-2. Markers (black) are as in Fig. 3*B*. (*D*) Structure of the C-terminus of PID-2 constrained by PAR-5. (*E*) Overlay of models predicted by AF 2 and AF 3 superimposed using PAR-5 showing similar interactions between the C-terminus of PID-2 (lime or red) and PAR-5 (magenta or green) although the rest of the PID-2 protein are positioned differently in the two models. Pseudobonds are as in Fig. 3*A*. Also see Movie S78.

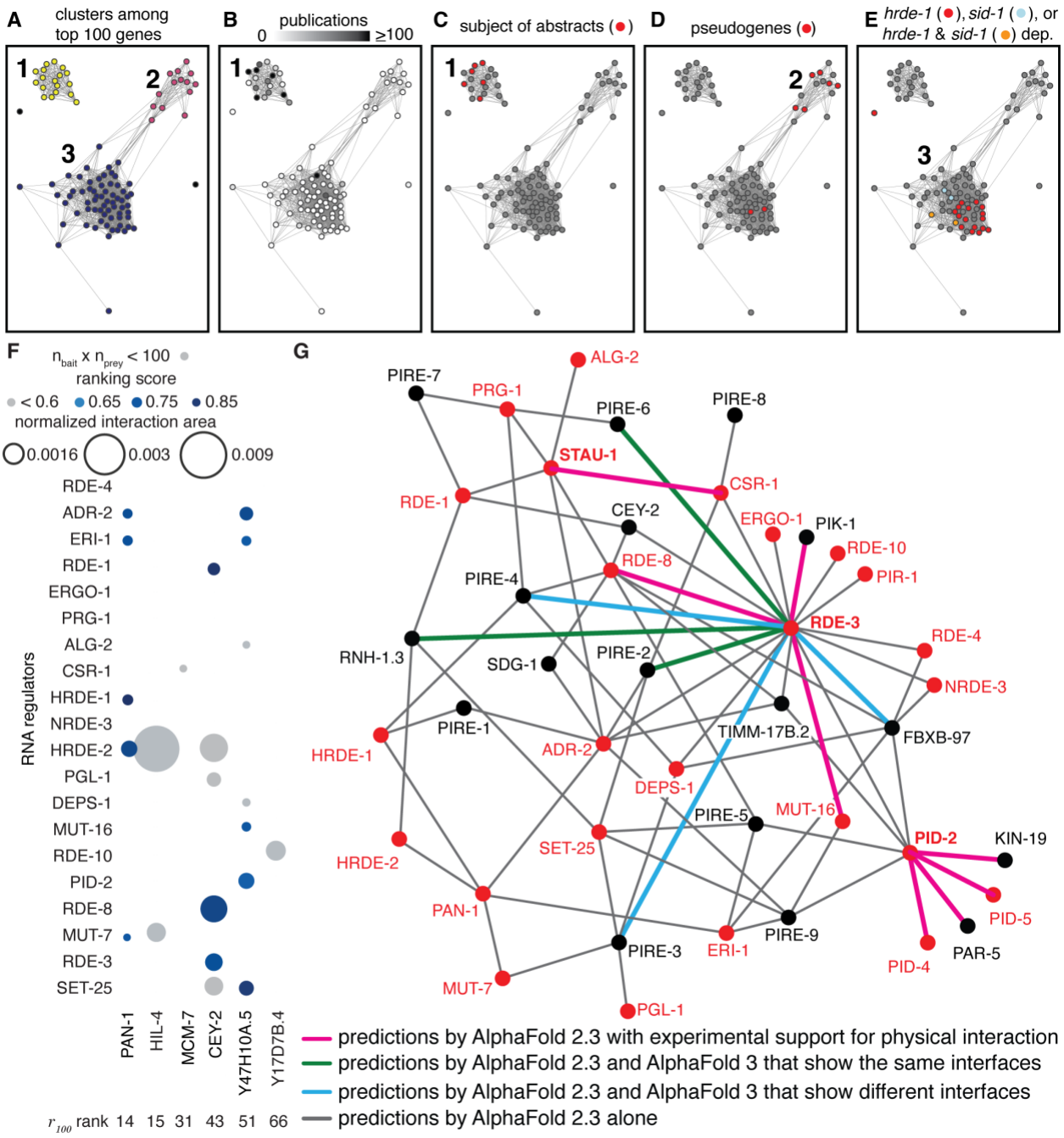

Figure 8. Clusters formed by understudied regulated genes suggest priorities for detailed study. (*A* to *E*) Properties of the top 100 regulated genes in the field of RNA silencing in *C. elegans.* (*A*) Clusters of genes based on their historical mutual information (HMI). Threshold for link: distance (1 - HMI) < 0.9. (*B* to *E*) Network in (*A*) with nodes colored to show number of publications per gene (white, 0; black, ≥100) (*B*), genes that have been the main subject of abstracts on RNA silencing in *C. elegans* (*C*), pseudogenes (red) (*D*), and genes changed in *hrde-1* mutants (69) (red), a *sid-1* mutant (16) (cyan), or both (orange) (*E*). (*F*) Predicted interactions of proteins encoded by genes with different r_{100} ranks with known regulators of RNA silencing. Sizes of circles indicate normalized interaction area and shading indicates ranking score. Grey indicates ranking scores < 0.6 and/or the products of numbers of constrained residues (n_{bait} x

n_{prey}) < 100. Also see Movies S80 to Movie S93. (*G*) All interactions (connecting lines) depicted were identified by AF 2 (grey). Some are supported by experimental evidence for physical interaction (magenta) and some are also predicted by AF 3 with either similar (green) or different (cyan) interfaces. Known regulators of RNA silencing are in red and those used as baits to look for predicted interactors (STAU-1, PID-2, and RDE-3) are in bold. Also see Table S4.

Supplementary Information

Selecting genes for analysis using historically contingent progress: from RNA changes to protein-protein interactions

Farhaan Lalit[1], Antony M Jose[1]*

Affiliations:

[1]University of Maryland, College Park, MD, USA.
*Corresponding author. Email: amjose@umd.edu

This file includes:

Supplementary Methods
SI References
7 Supplementary Figures
5 Supplementary Tables
94 Supplementary Movie Legends

Supplementary Methods

Analysis of gene data tables. To identify studies on RNA silencing in *C. elegans* with data tables that can be compared across all studies, we used the term 'C. elegans RNA silencing' to search PubMed. After examining the abstracts of more than 2000 studies that resulted from the search, the available data tables from 82 studies that were published between 2007 and 2022 were downloaded (Table S1), reformatted into 398 distinct tables manually and/or using custom scripts. Metadata if supplied by the authors for each table were retained as comments above each table. Gene names were unified using the Gene Name Sanitizer (https://wormbase.org/tools/mine/gene_sanitizer.cgi) as on 26 April 2022 (0_sanitization.py). It is unclear how an exhaustive list of papers that is nevertheless field-restricted could ever be defined for any field. Accordingly, our list of RNA silencing studies in *C. elegans* is not exhaustive and we apologize to colleagues whose work is not included in our analysis. Nevertheless, this effort captured additional datasets compared with those available in other more unrestricted collections that attempt to collect tables from all studies on an organism (e.g. WormExp 2.0 (1)). Only 30 of the 55 studies published before 2017 and included in this study overlapped with the 461 included in WormExp 2.0 as on 27 Jul 2017, which was available for download from the website (https://wormexp.zoologie.uni-kiel.de/wormexp/). This overlap was determined by comparing the paper IDs using a custom script (0_dataset_wormexp_overlap.ipynb). Data tables that reported p-values or adjusted p-values were filtered to only include entries with $p < 0.05$ (0_filter_pvals.py). Since fold-changes were not always available, for every dataset, genes were scored as present or absent (1_TableOccupancy.py) to generate a heatmap featuring the most frequently changed genes sorted by r_g values, where the number of genes considered (g) can be arbitrary (e.g., 25 in Fig. 1*F* and 100 in Fig. 8). The relationships between the parameters S_i, T_i, and g (Fig. 1*C*) were obtained using simulated data by sampling 100 random sets of genes (0_rg_simulation_box-whisker.ipynb) as the top g genes from a total of 20,000 genes and similarly sampling the genes in datasets of various sizes (T_i). For each gene in published lists in the field, the number of references listed on Wormbase (https://wormbase.org/) was used as a measure of the extent to which the gene has been studied (2_fig1D_r25_references.ipynb). Genes with fewer than 10 references were defined as understudied (Fig. 1*D*). To generate the heatmap (3_fig1F_fig1G_r25_related.ipynb, 4_heatmaps_normalized_100_full.ipynb), genes were ordered by decreasing values of r_{25} (top to bottom in Fig. 1*F*) and datasets were ordered by decreasing values of $\frac{S_i}{T_i}$. (left to right in Fig. 1*F*). To determine the co-occurrence patterns of all pairs of genes, Jaccard distances ($d_J = 1 - \frac{|X \cap Y|}{|X \cup Y|}$, where X and Y are sets of lists containing genes x and y, respectively) were calculated for each pair and all genes were hierarchically clustered using the 'average' linkage method. Relationships between genes based on occurrence in datasets were also captured as normalized mutual information (5_sklearn_nmi.ipynb) and defined as historical mutual information (HMI) to emphasize the dependence on the biased availability or inclusion of data based on historical progress in addition to the functional relatedness of the genes. Specifically, it was defined to be a symmetric and normalized mutual information score (2) and was calculated using the function normalized_mutual_info_score from scikit-learn (3) for genes X and Y:

$$HMI(X;Y) := \frac{2.MI(X;Y)}{H(X) + H(Y)},$$

where $MI(X;Y) = \sum_y \sum_x P_{(X,Y)}(x,y)\, log_2 \left(\frac{P_{(X,Y)}(x,y)}{P_X(x)P_Y(y)}\right)$, $H(X) = -\sum_x P(x) log_2\big(P(x)\big)$, and $H(Y) = -\sum_y P(y) log_2\big(P(y)\big)$. Mutual information (MI) determines how different the joint distribution of the gene pair (X, Y) is from the product of the marginal distributions of each gene, $H(X)$ and $H(Y)$ are the entropies of the two genes, and $P(\ldots)$ indicates probabilities. Clusters of genes based on HMI

values were identified using the Girvan-Newman algorithm (4). An interactive graphical user interface (GUI) for visualizing clusters and genes of interest (6_HMI_explorer.py) was created using Dash (Python) and figures highlighting genes within the clusters were generated (7_fig8.ipynb). Gene Ontology (GO) analysis was performed on all clusters using the Gene Ontology Resource ((5,6); https://geneontology.org/). Tables of the top 25 genes ranked by r_{25} when different numbers of total top genes are considered (Table S5) were generated for comparison (8_table_S5_r25_with_100_total.ipynb, 8_table_S5_r25_with_1000_total.ipynb).

Analysis of predicted protein structures. Predicted protein-protein interactions were examined using Alphafold 2.3.2 and the Alphafold 3 server, downloaded to a local machine, and analyzed using ChimeraX and custom scripts.

Alphafold 2. For each understudied regulated gene, files with protein sequences (.fasta) encoded by the longest transcript isoform were obtained from Wormbase and combined using the program 'fasta_assembly_for_alphafold_dimer.py' to create paired fasta files to be used for testing the potential for an interaction between the two proteins. Batches of potential interactors prepared in this way were run on the high-performance computing cluster (Zaratan, UMD) using a batch submission script ('alphafold_multimer_batch_submission.sh') that modifies another script for submitting alphafold 2.3.2 jobs with the model_preset flag set to 'multimer' ('alphafold_multimer.sh'). Typical resource requests included a wall time of 18 hours, one A100 GPU, and 8 CPUs at 6 GB each. Upon completion, a script for reducing the results folder to keep only the highest-ranking model was run ('alphafold_results_cleanup.sh') before downloading from the HPCC to a local machine. To analyze and annotate the downloaded models, the 'alphafold2_dimer_batch_computed_on_zaratan.py' program and run using the command 'chimerax --exit alphafold2_dimer_batch_computed_on_zaratan.py', which runs the python program within ChimeraX-1.7.1. Data for all predicted interactions to be analyzed together were collected under the same file ('yyyy_m_d_alphafold2_summary_stats'), where yyyy_m_d indicates date. This program also generated most of the supplemental movies. The program 'predicted_influencer_of_RNA_regulated_expression_d2.py' was then run to extract information about the interactions and make plots with either absolute interaction areas or areas normalized based on the sizes of the interacting proteins (passed to the program through the files ('yyyy_m_d_A_list_sizes' and 'yyyy_m_d_B_list_sizes'). Additional plots showing the residue numbers and locations of residues interacting with each regulator were created using the program 'interactor_map_for_a_protein_with_another_set_of_proteins.py'. The final figure showing the scaled area of interaction shaded according to the ranking score (Fig. 2*B*) was generated using 'final_interactors_filtered_by_model_rankings.py'.

Analysis of Alphafold 2 models using chimeraX and the downstream computations can also be performed using the two scripts 'predicted_dimer_chimerax.py' and 'predicted_dimer_python.py'. These streamlined scripts also generate distributions of the ranking scores for the 25 models identified with each run of Alphafold 2.

Alphafold 3. Essentially the same workflow as above was used after downloading the predicted interactions for pairs of proteins from the Alphafold 3 server, which was run in batches of 10 or 20 per day based on quota availability. Parsing the resulting data required some minor modifications to the programs because the error files (.json) and the structure files (.cif) were in different formats and labeled differently. The program 'alphafold3_dimer_batch_computed_on_google.py' was used for analyzing these predictions.

Comparisons of Alphafold 2 and Alphafold 3. For comparisons of the two prediction approaches, the 'alphafold3_dimer_batch_computed_on_google_comparing_af2_af3.py', 'predicted_influencer_of_RNA_regulated_expression_d2_af2_vs_af3_af3_run.py' and 'interactor_map_for_a_protein_with_another_set_of_proteins_comparing_af2_vs_af3_rerun_on_af3.py' programs were used.

Illustrations. Illustrations of protein-protein complexes for figures were created manually using ChimeraX (1.7.1 or 1.8-rc2024.05.24) and Adobe Illustrator (28.5). Typical workflow on ChimeraX included opening the .pdb or .cif files and the associated predicted aligned error files (.json or .pkl), aligning them as necessary, coloring different proteins, overlaying multiple models when relevant, and adding inter-protein pseudobonds based on criteria before saving images and/or movies. All interactions predicted in the study were summarized using Gephi (v. 0.10.1 202301172018) and Adobe Illustrator (v. 28.7.1).

Supplementary Figures

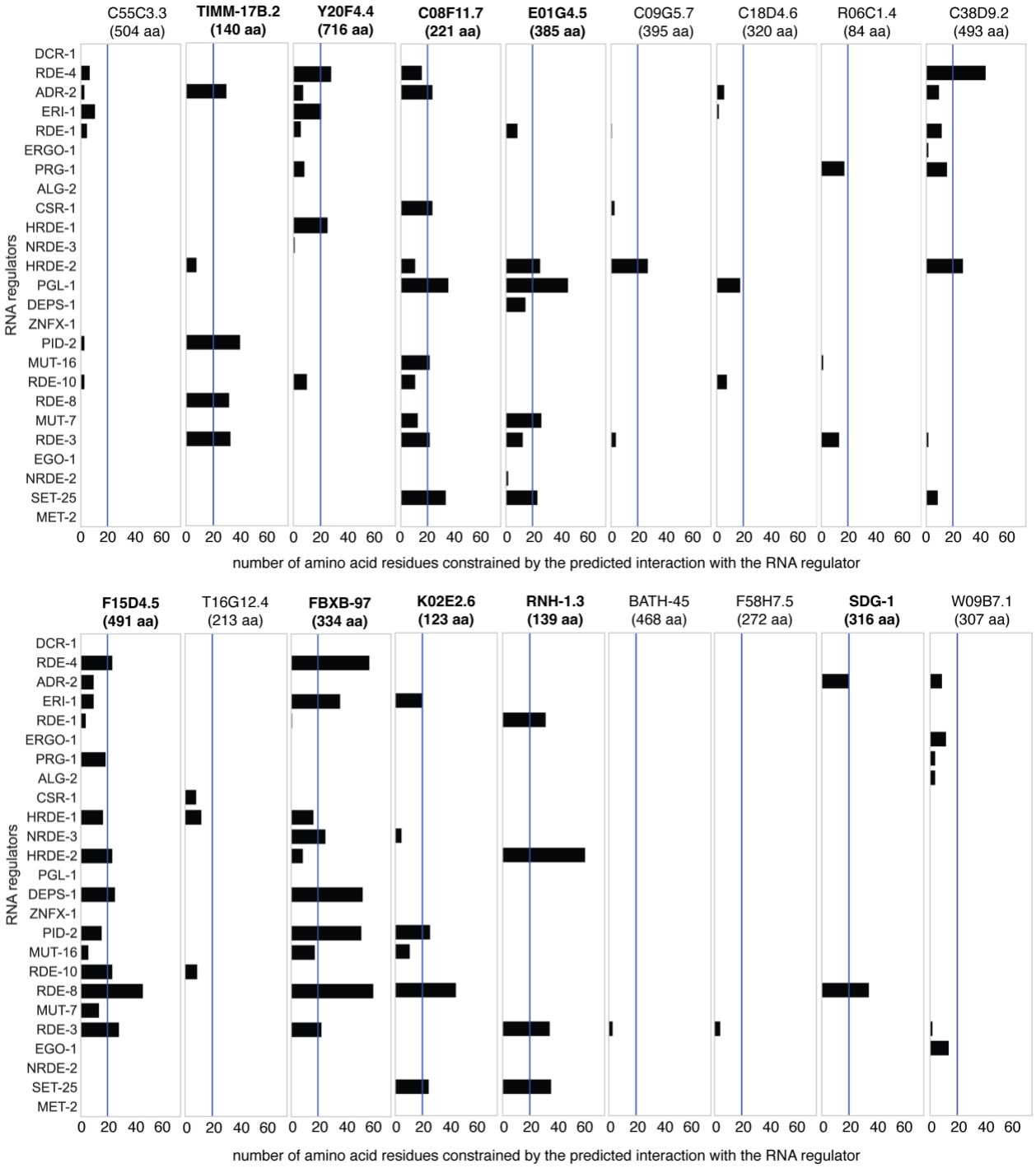

Figure S1. Numbers of candidate PIRE protein residues constrained by the predicted interacting regulator of RNA silencing in *C. elegans*. Numbers of residues that interact with an inter-protein PAE < 5Å and a distance between residues < 6Å are plotted for each interaction between a protein encoded by an understudied gene and a known regulator of RNA silencing in *C. elegans*. A threshold of 20 residues (blue line) and a ranking score >0.6 was used to separate candidate PIRE proteins (highlighted in bold) from others encoded by understudied genes.

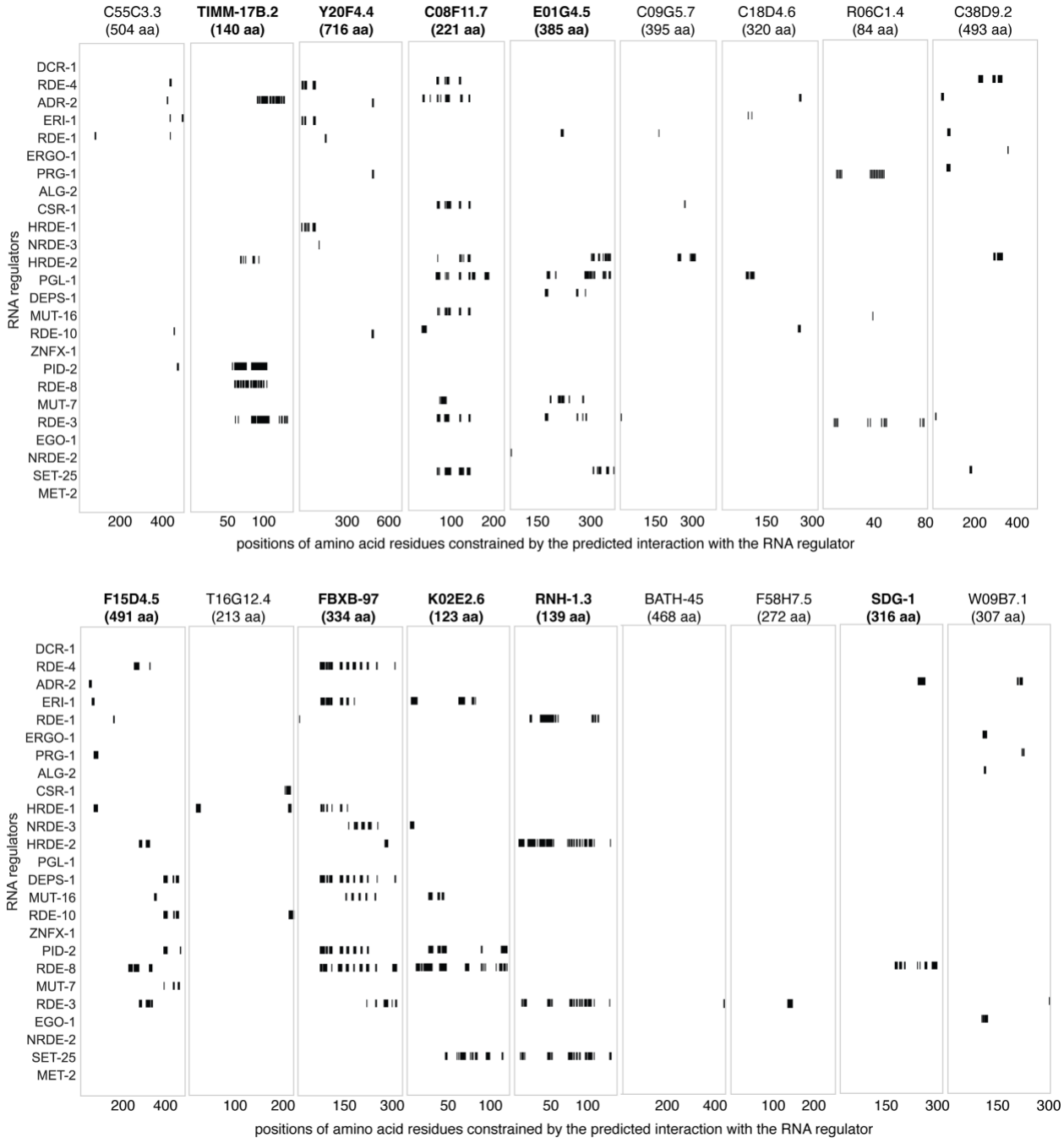

Figure S2. Regions of the candidate PIRE protein sequence constrained by the predicted interacting regulator of RNA silencing in *C. elegans*. Markers (black) are enlarged with respect to the X-axis for visibility (e.g., the marker denoting the interaction between RDE-1 and FBXB-97 only indicates one residue). Understudied genes that encode candidate PIRE proteins are highlighted in bold.

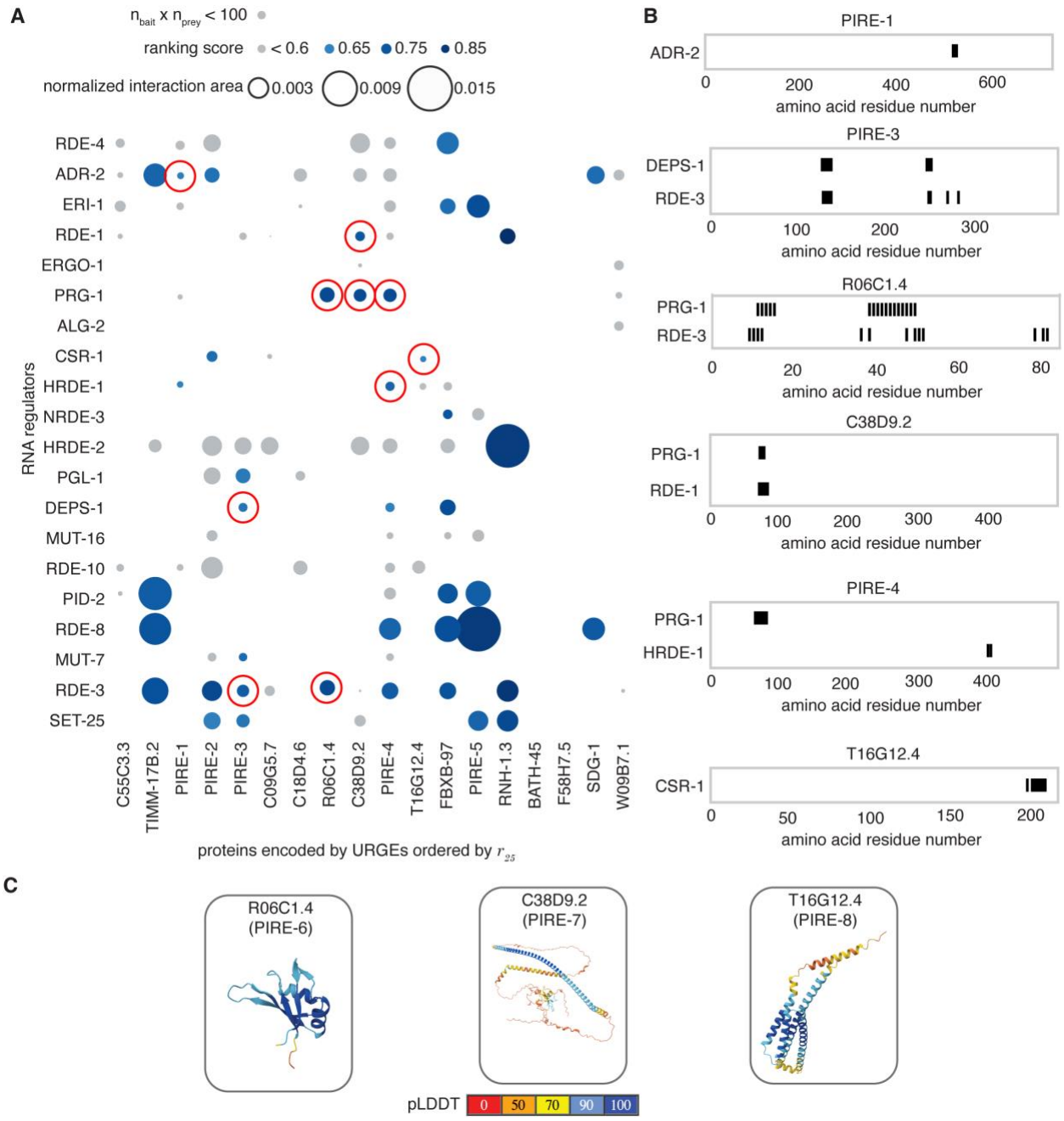

Figure S3. Predicted interactions between proteins encoded by the top 25 genes and known regulators of RNA silencing identified with more permissive criteria. (*A*) The area of the interaction surface between partners normalized by the product of the sizes of the interactors is shown as a bubble plot. Interactions are shaded according to ranking score. Interactions for which the product of the numbers of interacting residues (n_{bait} x n_{prey}) with an inter-protein predicted aligned error < 5Å and inter-residue distance < 6Å in a model with a ranking score > 0.6 is less than 100 are shaded grey. Ten interactions identified in addition to those found using criteria in Fig. 2*B* are highlighted with red circles. (*B*) Regions of the additionally identified proteins constrained by the interacting regulators (red circles in *A*) with markers depicted as in Fig. 3*B*. (*C*) Predicted structures for additional PIRE proteins with pLDDT as in Fig. 2*D*. Also see Movies S39 to S48.

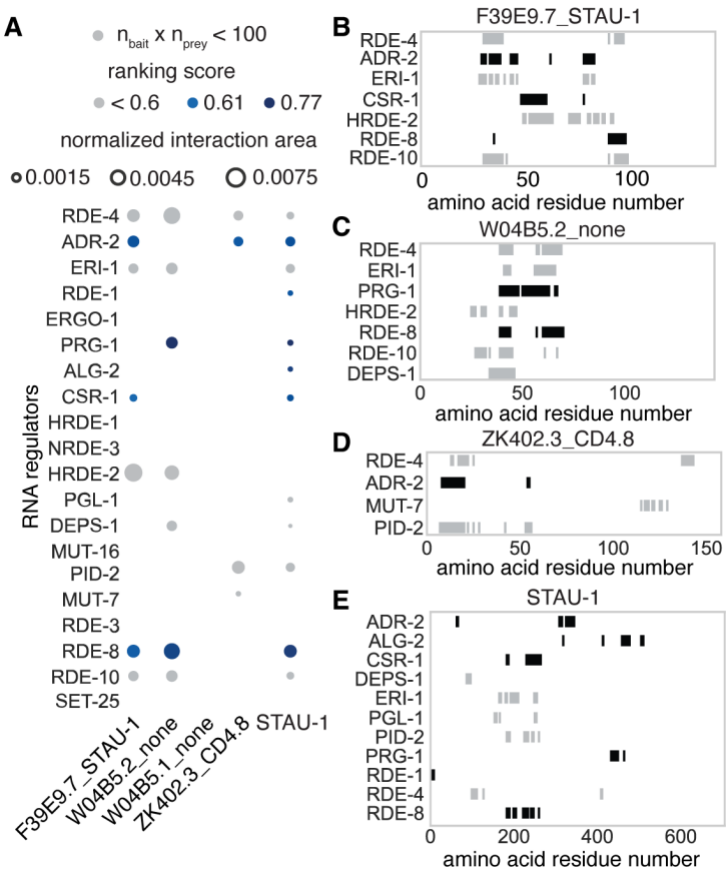

Figure S4. Predicted interactions of potential peptides encoded by pseudogenes and a homologous protein with regulators of RNA silencing. (*A*) Interactions are depicted as in Fig. S3*A*. The proteins are labeled with their closest BLAST matches separated by an underscore (e.g., F39E9.7_STAU-1 indicates that the peptide that could be encoded by F39E9.7 shares homology with STAU-1). (*B* to *D*) Regions of the longest peptide sequences encoded by F39E9.7 (*B*), W04B5.2 (*C*), and ZK402.3 (*D*) constrained by the interactors are shown with markers as in Fig. 3*B*. (*E*) Regions of STAU-1 protein sequence constrained by interacting regulators of RNA silencing are shown with markers as in Fig. 3*B*. Also see Movies S49 to S60.

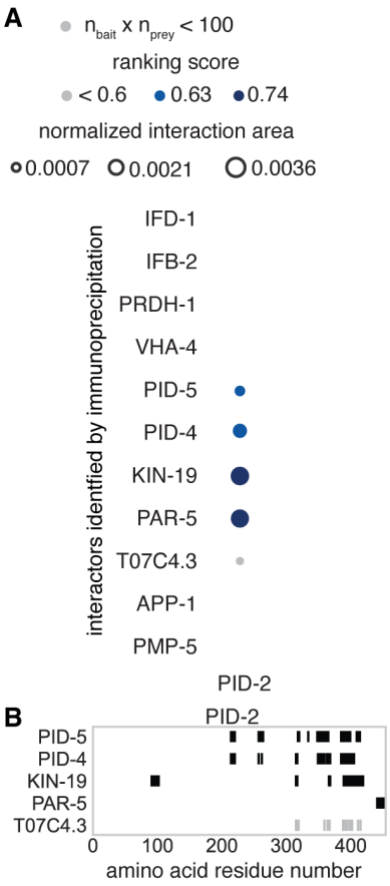

Figure S5. Predicted interactions between PID-2/ZSP-1 and proteins identified in a pulldown of PID-2 (as reported in (7)). (*A*) Interactions are depicted as in Fig. S3*A*. (*B*) Regions of the PID-2 protein sequence constrained by the interactors are shown with markers as in Fig. 3*B*. Also see Movies S73 to S77.

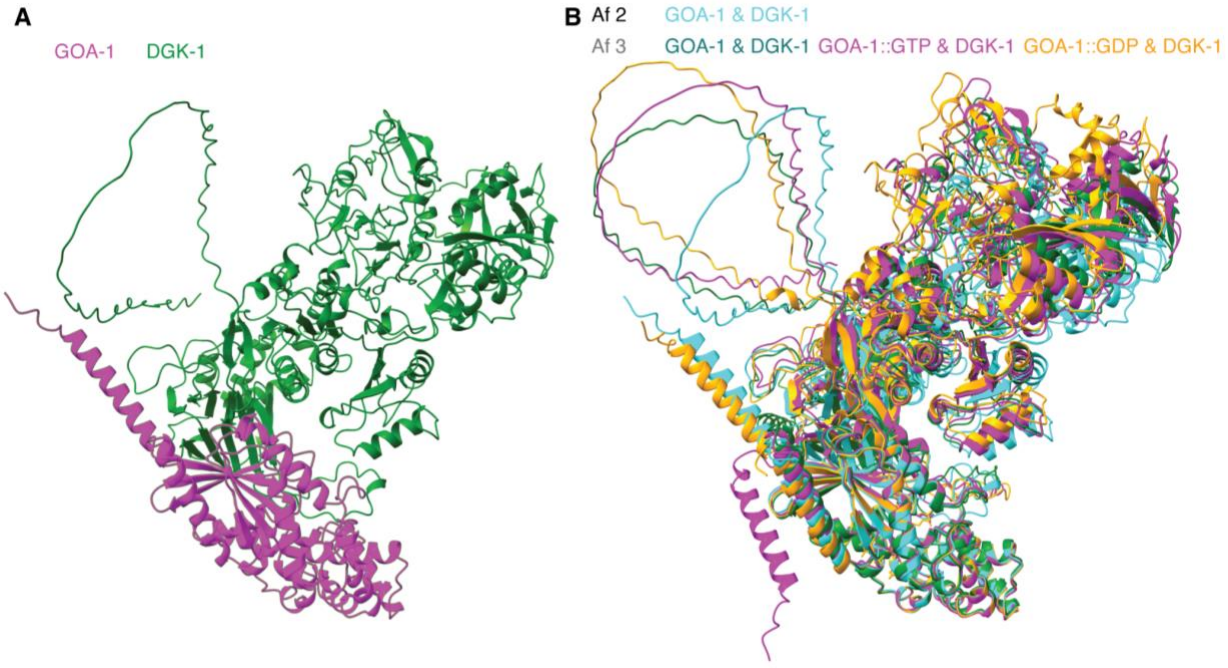

Figure S6. Interactions between the G alpha protein GOA-1 and the diacylglycerol kinase DGK-1 predicted by AlphaFold. (*A*) Interaction between GOA-1 (magenta) and DGK-1 (green) predicted by AlphaFold 2. (*B*) Overlay of the GOA-1::DGK-1 complex predicted by AlphaFold 2 (cyan) with those predicted by the AlphaFold 3 server (green, magenta, and orange for free, GTP-bound, and GDP-bound GOA-1, respectively). Also see Movie S79.

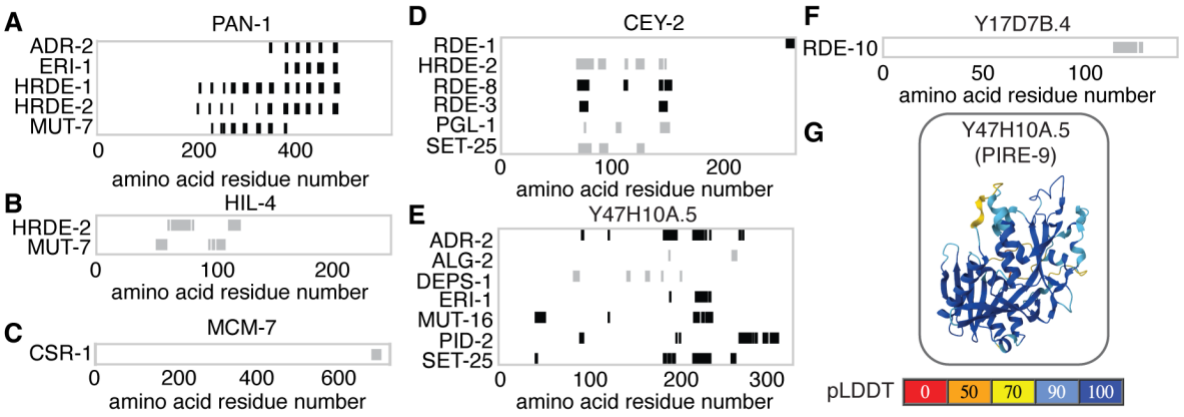

Figure S7. A sampling of predicted interactions between regulators of RNA silencing and proteins encoded by the top 100 genes with varying r_{100} ranks. (*A* to *F*) Regions of the PAN-1 (*A*), HIL-4 (*B*), MCM-7 (*C*), CEY-2 (*D*), Y47H10A.5 (*E*), and Y17D7B.4 (*F*) protein sequences constrained by the interactors are shown with markers as in Fig. 3B. Also see Movies S80 to S93. (*G*) Predicted structures for an additional PIRE protein with pLDDT as in Fig. 2*D*. Also see Fig. 8*F*.

Tables and Table Legends

Table S1. Data tables used in this study. List of the 398 tables used along with links to the 82 studies from which they were taken and a brief description of the data types. See excel file.

Table S2. Top 100 genes grouped according to historical mutual information (HMI). List of genes within clusters formed by the top 100 genes with distance (1 – HMI) < 0.9. The two genes that are not part of any clusters are listed as singletons.

Cluster 1	Cluster 2	Cluster 3	Singletons
csr-1	F39F10.4	*gpx-8*	R03D7.2
tbb-2	H09G03.1	F40D4.13	*pyk-1*
hsp-1	W04B5.1	*dyf-3*	
cey-2	Y47H10A.5	C46G7.5	
pgl-3	Y17D7B.4	*citk-1*	
hrde-1	F39E9.7	Y57G11C.51	
mcm-7	ZK402.3	*saeg-2*	
klp-15	E01G4.5	F09C8.2	
par-5	W04B5.2	*gly-13*	
klp-7	W05H12.2	*fbxb-97*	
cdk-1	K02E2.6	Y20F4.4	
hil-4	Y37E11B.2	ZK973.8	
wago-1	Y105C5A.14	*spch-1*	
hsp-90	F55C9.3	Y57G7A.5	
cpg-1		*pan-1*	
rme-2		W09B7.1	
wago-4		*elf-1*	
tba-2		C38C3.3	
		T20F7.1	
		fkb-8	
		K05C4.9	
		F15D4.5	
		sea-2	
		F55B11.6	
		F41G4.7	
		T16G12.8	
		C30G12.1	
		saeg-1	
		rnh-1.3	
		Y53F4B.5	
		E02H9.3	
		his-24	
		ZK909.3	

vet-6
C04G6.6
lin-15B
qdpr-1
W09B7.2
K09H9.7
T02G5.4
lido-18
T11F9.10
scrm-4
clp-6
C08F11.7
pdfr-1
F58H7.5
T16G12.4
C09G5.7
Y48G1BM.6
C18D4.6
ZK795.2
ceh-20
W05F2.4
bath-13
timm-17B.2
fbxa-192
R03H10.6
bath-45
C55C3.3
R06C1.4
C38D9.2
T03D3.5
glit-1
mif-2
spe-41

Table S3. Gene Ontology terms associated with genes in Cluster 1 among the top 100 genes clustered using historical mutual information.

GO term	# in set	# identified	# expected	Enrichment	P value
regulation of biological process	4202	13	4.03	3.23	3.20E-02
developmental process	1846	10	1.77	5.65	5.10E-03

cellular component organization	1830	10	1.75	5.7	4.70E-03
cellular component organization or biogenesis	1982	10	1.9	5.26	9.78E-03
anatomical structure development	1696	9	1.63	5.54	2.55E-02
regulation of macromolecule metabolic process	1646	9	1.58	5.71	1.99E-02
regulation of metabolic process	1745	9	1.67	5.38	3.22E-02
cell cycle process	400	9	0.38	23.48	9.93E-08
cell cycle	517	9	0.5	18.16	9.66E-07
negative regulation of biological process	962	8	0.92	8.68	3.55E-03
reproductive process	803	8	0.77	10.4	9.01E-04
sexual reproduction	425	8	0.41	19.64	6.51E-06
cell differentiation	824	8	0.79	10.13	1.10E-03
cellular developmental process	826	8	0.79	10.11	1.12E-03
mitotic cell cycle	269	8	0.26	31.03	1.74E-07
organelle organization	1091	8	1.05	7.65	9.11E-03
negative regulation of cellular process	854	7	0.82	8.55	2.18E-02
mitotic cell cycle process	233	7	0.22	31.35	3.21E-06
embryo development	516	7	0.49	14.16	7.57E-04
regulation of cell cycle	245	6	0.23	25.55	2.01E-04
multicellular organismal reproductive process	384	6	0.37	16.3	2.82E-03
regulation of cell cycle process	185	5	0.18	28.2	1.78E-03
gamete generation	254	5	0.24	20.54	8.45E-03
germ cell development	176	5	0.17	29.64	1.39E-03
cellular process involved in reproduction in multicellular organism	178	5	0.17	29.31	1.47E-03
microtubule cytoskeleton organization	202	5	0.19	25.83	2.74E-03
microtubule-based process	281	5	0.27	18.57	1.38E-02
embryo development ending in birth or egg hatching	303	5	0.29	17.22	2.00E-02
regulatory ncRNA-mediated gene silencing	109	4	0.1	38.29	7.97E-03
regulation of mitotic cell cycle	94	4	0.09	44.4	4.41E-03

oogenesis	117	4	0.11	35.67	1.06E-02
female gamete generation	144	4	0.14	28.99	2.41E-02
nuclear chromosome segregation	121	4	0.12	34.49	1.21E-02
chromosome segregation	155	4	0.15	26.93	3.22E-02
nuclear division	166	4	0.16	25.14	4.22E-02

Table S4. Potential hypotheses for the function(s) of PIRE proteins without common names. Function(s) of the known regulators of RNA silencing could be promoted or inhibited by interacting PIRE proteins.

PIRE	Interactor	Known function(s) of RNA regulator(s)
PIRE-1/ Y20F4.4	ADR-2	A-to-I editing of dsRNA (double-stranded RNA) (8)
	HRDE-1	Argonaute activity (9)
PIRE-2/ C08F11.7	ADR-2	A-to-I editing of dsRNA (double-stranded RNA) (8)
	CSR-1	Argonaute activity (10)
	RDE-3	poly-UG RNA production (11,12)
	SET-25	histone methyltransferase activity (13,14)
PIRE-3/ E01G4.5	DEPS-1	germ granule formation and/or RNA silencing (15)
	RDE-3	poly-UG RNA production (11,12)
	PGL-1	mRNA regulation and/or P granule formation (16)
	MUT-7	3'-5' exoribonuclease activity (17)
	SET-25	histone methyltransferase activity (13,14)
PIRE-4/ F15D4.5	DEPS-1	germ granule formation and/or RNA silencing (15)
	HRDE-1	Argonaute activity (9)
	PRG-1	Argonaute activity (18)
	RDE-8	RNA endonuclease and/or mRNA binding activity (19)
	RDE-3	poly-UG RNA production (11,12)
PIRE-5/ K02E2.6	ERI-1	3'-5' exoribonuclease activity (20)
	PID-2	piRNA-mediated silencing and/or Z-granule formation (7)
	RDE-8	RNA endonuclease and/or mRNA binding activity (19)
	SET-25	histone methyltransferase activity (13,14)
PIRE-6/ R06C1.4	RDE-3	poly-UG RNA production (11,12)
	PRG-1	Argonaute activity (18)
PIRE-7/ C38D9.2	RDE-1	Argonaute activity (21,22)
	PRG-1	Argonaute activity (18)
PIRE-8/ T16G12.4	CSR-1	Argonaute activity (10)
PIRE-9/ Y47H10A.5	ADR-2	A-to-I editing of dsRNA (8)
	ERI-1	3'-5' exoribonuclease activity (20)
	PID-2	piRNA-mediated silencing and/or Z-granule formation (7)
	MUT-16	secondary small RNA production and mutator foci formation (23)
	SET-25	histone methyltransferase activity (13,14)

Table S5. r_g rank order of frequently identified genes. Top 25 rank-ordered genes obtained by calculating r_g using 25, 100, or 1000 of the most frequently listed genes among the 398 tables considered in this study. In bold are genes shared with the top 25 identified using the most frequent 1000 genes.

r_{25} genes		r_{100} genes		r_{1000} genes	
C55C3.3	0.0164	**C55C3.3**	0.0164	**C55C3.3**	0.0164
timm-17B.2	0.0149	***timm-17B.2***	0.0149	***timm-17B.2***	0.0149
Y20F4.4	0.0135	**Y20F4.4**	0.0135	**Y20F4.4**	0.0135
C08F11.7	0.0125	**C08F11.7**	0.0125	**C08F11.7**	0.0125
E01G4.5	0.0120	**E01G4.5**	0.0120	**E01G4.5**	0.0120
ZK402.3	0.0119	**ZK402.3**	0.0119	**ZK402.3**	0.0119
C09G5.7	0.0118	**C09G5.7**	0.0118	**C09G5.7**	0.0118
hrde-1	0.0117	***hrde-1***	0.0117	***hrde-1***	0.0117
C18D4.6	0.0117	**C18D4.6**	0.0117	**C18D4.6**	0.0117
R06C1.4	0.0116	**R06C1.4**	0.0116	**R06C1.4**	0.0116
C38D9.2	0.0115	**C38D9.2**	0.0115	**C38D9.2**	0.0115
F15D4.5	0.0115	**F15D4.5**	0.0115	**F15D4.5**	0.0115
T16G12.4	0.0109	**Y57G11C.51**	0.0112	**Y57G11C.51**	0.0112
fbxb-97	0.0107	***pan-1***	0.0111	***pan-1***	0.0111
W04B5.1	0.0103	***hil-4***	0.0111	***hil-4***	0.0111
spe-41	0.0102	***cdk-1***	0.0111	***cdk-1***	0.0111
scrm-4	0.0098	**T16G12.4**	0.0109	**T16G12.4**	0.0109
F39E9.7	0.0098	***fbxb-97***	0.0107	***fbxb-97***	0.0107
K02E2.6	0.0097	**F39F10.4**	0.0106	**F39F10.4**	0.0106
W04B5.2	0.0096	**K09H9.7**	0.0106	**K09H9.7**	0.0106
rnh-1.3	0.0095	***tbb-2***	0.0105	***tbb-2***	0.0105
bath-45	0.0094	***saeg-1***	0.0105	***saeg-1***	0.0105
F58H7.5	0.0084	**W04B5.1**	0.0103	**W04B5.1**	0.0103
SDG-1	0.0062	***spe-41***	0.0102	***spe-41***	0.0102
W09B7.1	0.0032	***csr-1***	0.0101	***csr-1***	0.0101

Supplementary Movie Legends

Movie S1. TIMM-17B.2 and ADR-2 with inter-protein predicted aligned error < 5 and distance < 6
Movie S2. TIMM-17B.2 and PID-2 with inter-protein predicted aligned error < 5 and distance < 6
Movie S3. TIMM-17B.2 and RDE-8 with inter-protein predicted aligned error < 5 and distance < 6
Movie S4. TIMM-17B.2 and RDE-3 with inter-protein predicted aligned error < 5 and distance < 6
Movie S5. Y20F4.4 and HRDE-1 with inter-protein predicted aligned error < 5 and distance < 6
Movie S6. C08F11.7 and ADR-2 with inter-protein predicted aligned error < 5 and distance < 6
Movie S7. C08F11.7 and CSR-1 with inter-protein predicted aligned error < 5 and distance < 6
Movie S8. C08F11.7 and RDE-3 with inter-protein predicted aligned error < 5 and distance < 6
Movie S9. C08F11.7 and SET-25 with inter-protein predicted aligned error < 5 and distance < 6
Movie S10. E01G4.5 and PGL-1 with inter-protein predicted aligned error < 5 and distance < 6
Movie S11. E01G4.5 and MUT-7 with inter-protein predicted aligned error < 5 and distance < 6

Movie S12. E01G4.5 and SET-25 with inter-protein predicted aligned error < 5 and distance < 6
Movie S13. F15D4.5 and DEPS-1 with inter-protein predicted aligned error < 5 and distance < 6
Movie S14. F15D4.5 and RDE-8 with inter-protein predicted aligned error < 5 and distance < 6
Movie S15. F15D4.5 and RDE-3 with inter-protein predicted aligned error < 5 and distance < 6
Movie S16. FBXB-97 and RDE-4 with inter-protein predicted aligned error < 5 and distance < 6
Movie S17. FBXB-97 and ERI-1 with inter-protein predicted aligned error < 5 and distance < 6
Movie S18. FBXB-97 and NRDE-3 with inter-protein predicted aligned error < 5 and distance < 6
Movie S19. FBXB-97 and DEPS-1 with inter-protein predicted aligned error < 5 and distance < 6
Movie S20. FBXB-97 and PID-2 with inter-protein predicted aligned error < 5 and distance < 6
Movie S21. FBXB-97 and RDE-8 with inter-protein predicted aligned error < 5 and distance < 6
Movie S22. FBXB-97 and RDE-3 with inter-protein predicted aligned error < 5 and distance < 6
Movie S23. K02E2.6 and ERI-1 with inter-protein predicted aligned error < 5 and distance < 6
Movie S24. K02E2.6 and PID-2 with inter-protein predicted aligned error < 5 and distance < 6
Movie S25. K02E2.6 and RDE-8 with inter-protein predicted aligned error < 5 and distance < 6
Movie S26. K02E2.6 and SET-25 with inter-protein predicted aligned error < 5 and distance < 6
Movie S27. RNH-1.3 and RDE-1 with inter-protein predicted aligned error < 5 and distance < 6
Movie S28. RNH-1.3 and HRDE-2 with inter-protein predicted aligned error < 5 and distance < 6
Movie S29. RNH-1.3 and RDE-3 with inter-protein predicted aligned error < 5 and distance < 6
Movie S30. RNH-1.3 and SET-25 with inter-protein predicted aligned error < 5 and distance < 6
Movie S31. SDG-1 and ADR-2 with inter-protein predicted aligned error < 5 and distance < 6
Movie S32. SDG-1 and RDE-8 with inter-protein predicted aligned error < 5 and distance < 6
Movie S33. RNH-1.3 and RDE-3 predicted by AlphaFold 2 versus the AlphaFold 3 server
Movie S34. FBXB-97 and RDE-3 predicted by AlphaFold 2 versus the AlphaFold 3 server
Movie S35. PIRE-4 and RDE-3 predicted by AlphaFold 2 versus the AlphaFold 3 server
Movie S36. EGO-1 and W09B7.1 predicted by AlphaFold 2 versus the AlphaFold 3 server
Movie S37. Overlay of two models for the RNH-1.3:RDE-3 complex predicted by AlphaFold 2.
Movie S38. Overlay of two models for the RNH-1.3:RDE-3 complex predicted by AlphaFold 3.
Movie S39. PIRE-1 and RDE-1 with inter-protein predicted aligned error < 5 and distance < 6.
Movie S40. DEPS-1 and PIRE-3 with inter-protein predicted aligned error < 5 and distance < 6.
Movie S41. RDE-3 and PIRE-3 with inter-protein predicted aligned error < 5 and distance < 6.
Movie S42. R06C1.4 and PRG-1 with inter-protein predicted aligned error < 5 and distance < 6.
Movie S43. R06C1.4 and RDE-3 with inter-protein predicted aligned error < 5 and distance < 6.
Movie S44. C38D9.2 and RDE-1 with inter-protein predicted aligned error < 5 and distance < 6.
Movie S45. C38D9.2 and PRG-1 with inter-protein predicted aligned error < 5 and distance < 6.
Movie S46. PRG-1 and PIRE-4 with inter-protein predicted aligned error < 5 and distance < 6.
Movie S47. HRDE-1 and PIRE-4 with inter-protein predicted aligned error < 5 and distance < 6.
Movie S48. T16G12.4 and CSR-1 with inter-protein predicted aligned error < 5 and distance < 6.
Movie S49. ADR-2 and the longest peptide that could be encoded by F39E9.7 with inter-protein predicted aligned error < 5 and distance < 6.
Movie S50. CSR-1 and the longest peptide that could be encoded by F39E9.7 with inter-protein predicted aligned error < 5 and distance < 6.
Movie S51. RDE-8 and the longest peptide that could be encoded by F39E9.7 with inter-protein predicted aligned error < 5 and distance < 6.
Movie S52. PRG-1 and the longest peptide that could be encoded by W04B5.2 with inter-protein predicted aligned error < 5 and distance < 6.
Movie S53. RDE-8 and the longest peptide that could be encoded by W04B5.2 with inter-protein predicted aligned error < 5 and distance < 6.

Movie S54. ADR-2 and the longest peptide that could be encoded by ZK402.3 with inter-protein predicted aligned error < 5 and distance < 6.
Movie S55. ADR-2 and STAU-1 with inter-protein predicted aligned error < 5 and distance < 6.
Movie S56. RDE-1 and STAU-1 with inter-protein predicted aligned error < 5 and distance < 6.
Movie S57. PRG-1 and STAU-1 with inter-protein predicted aligned error < 5 and distance < 6.
Movie S58. ALG-2 and STAU-1 with inter-protein predicted aligned error < 5 and distance < 6.
Movie S59. CSR-1 and STAU-1 with inter-protein predicted aligned error < 5 and distance < 6.
Movie S60. RDE-8 and STAU-1 with inter-protein predicted aligned error < 5 and distance < 6.
Movie S61. ADR-2 and RDE-3 with inter-protein predicted aligned error < 5 and distance < 6.
Movie S62. CSR-1 and RDE-3 with inter-protein predicted aligned error < 5 and distance < 6.
Movie S63. DEPS-1 and RDE-3 with inter-protein predicted aligned error < 5 and distance < 6.
Movie S64. ERGO-1 and RDE-3 with inter-protein predicted aligned error < 5 and distance < 6.
Movie S65. MUT-16 and RDE-3 with inter-protein predicted aligned error < 5 and distance < 6.
Movie S66. NRDE-3 and RDE-3 with inter-protein predicted aligned error < 5 and distance < 6.
Movie S67. PID-2 and RDE-3 with inter-protein predicted aligned error < 5 and distance < 6.
Movie S68. PIK-1 and RDE-3 with inter-protein predicted aligned error < 5 and distance < 6.
Movie S69. PIR-1 and RDE-3 with inter-protein predicted aligned error < 5 and distance < 6.
Movie S70. RDE-4 and RDE-3 with inter-protein predicted aligned error < 5 and distance < 6.
Movie S71. RDE-8 and RDE-3 with inter-protein predicted aligned error < 5 and distance < 6.
Movie S72. RDE-10 and RDE-3 with inter-protein predicted aligned error < 5 and distance < 6.
Movie S73. PID-5 and PID-2 with inter-protein predicted aligned error < 5 and distance < 6.
Movie S74. PID-4 and PID-2 with inter-protein predicted aligned error < 5 and distance < 6.
Movie S75. KIN-19 and PID-2 with inter-protein predicted aligned error < 5 and distance < 6.
Movie S76. PAR-5 and PID-2 with inter-protein predicted aligned error < 5 and distance < 6.
Movie S77. T07C4.3 and PID-2 with inter-protein predicted aligned error < 5 and distance < 6.
Movie S78. Overlay of models for the PAR-5:PID-2 complex predicted by AlphaFold 2 and AlphaFold 3.
Movie S79. Overlay of models for the GOA-1:DGK-1 complexes predicted by AlphaFold 2 and AlphaFold 3.
Movie S80. CSR-1 and MCM-7 with inter-protein predicted aligned error < 5 and distance < 6.
Movie S81. ADR-2 and PAN-1 with inter-protein predicted aligned error < 5 and distance < 6.
Movie S82. ERI-1 and PAN-1 with inter-protein predicted aligned error < 5 and distance < 6.
Movie S83. HRDE-1 and PAN-1 with inter-protein predicted aligned error < 5 and distance < 6.
Movie S84. HRDE-2 and PAN-1 with inter-protein predicted aligned error < 5 and distance < 6.
Movie S85. MUT-7 and PAN-1 with inter-protein predicted aligned error < 5 and distance < 6.
Movie S86. RDE-1 and CEY-2 with inter-protein predicted aligned error < 5 and distance < 6.
Movie S87. RDE-8 and CEY-2 with inter-protein predicted aligned error < 5 and distance < 6.
Movie S88. RDE-3 and CEY-2 with inter-protein predicted aligned error < 5 and distance < 6.
Movie S89. Y47H10A.5 and ADR-2 with inter-protein predicted aligned error < 5 and distance < 6
Movie S90. Y47H10A.5 and ERI-1 with inter-protein predicted aligned error < 5 and distance < 6.
Movie S91. Y47H10A.5 and MUT-16 with inter-protein predicted aligned error < 5 and distance < 6
Movie S92. Y47H10A.5 and PID-2 with inter-protein predicted aligned error < 5 and distance < 6
Movie S93. Y47H10A.5 and SET-25 with inter-protein predicted aligned error < 5 and distance < 6
Movie S94. Simulation illustrating the growth of networks through preferential attachment (Screen capture of ‘Preferential Attachment Simple’ from NetLogo model library).

SI References

1. Yang, W., Dierking, K. and Schulenburg, H. (2016) WormExp: a web-based application for a Caenorhabditis elegans-specific gene expression enrichment analysis. *Bioinformatics*, **32**, 943-945.
2. Witten, I.H. and Frank, E. (2005) *Data Mining: Practical Machine Learning Tools and Techniques*. 2nd ed. Morgan Kaufmann, San Francisco.
3. Pedregosa, F., Varoquaux, G., Gramfort, A., Michel, V., Thirion, B., Grisel, O., Blondel, M., Prettenhofer, P., Weiss, R., Dubourg, V. *et al.* (2011) Scikit-learn: Machine Learning in Python. *Journal of Machine Learning Research*, **12**, 2825-2830.
4. Girvan, M. and Newman, M.E. (2002) Community structure in social and biological networks. *Proc Natl Acad Sci U S A*, **99**, 7821-7826.
5. Ashburner, M., Ball, C.A., Blake, J.A., Botstein, D., Butler, H., Cherry, J.M., Davis, A.P., Dolinski, K., Dwight, S.S., Eppig, J.T. *et al.* (2000) Gene ontology: tool for the unification of biology. The Gene Ontology Consortium. *Nat Genet*, **25**, 25-29.
6. Consortium, G.O., Aleksander, S.A., Balhoff, J., Carbon, S., Cherry, J.M., Drabkin, H.J., Ebert, D., Feuermann, M., Gaudet, P., Harris, N.L. *et al.* (2023) The Gene Ontology knowledgebase in 2023. *Genetics*, **224**, iyad031.
7. Placentino, M., de Jesus Domingues, A.M., Schreier, J., Dietz, S., Hellmann, S., de Albuquerque, B.F., Butter, F. and Ketting, R.F. (2021) Intrinsically disordered protein PID-2 modulates Z granules and is required for heritable piRNA-induced silencing in the Caenorhabditis elegans embryo. *EMBO J*, **40**, e105280.
8. Knight, S.W. and Bass, B.L. (2002) The role of RNA editing by ADARs in RNAi. *Mol Cell*, **10**, 809-817.
9. Buckley, B.A., Burkhart, K.B., Gu, S.G., Spracklin, G., Kershner, A., Fritz, H., Kimble, J., Fire, A. and Kennedy, S. (2012) A nuclear Argonaute promotes multigenerational epigenetic inheritance and germline immortality. *Nature*, **489**, 447-451.
10. Claycomb, J.M., Batista, P.J., Pang, K.M., Gu, W., Vasale, J.J., van Wolfswinkel, J.C., Chaves, D.A., Shirayama, M., Mitani, S., Ketting, R.F. *et al.* (2009) The Argonaute CSR-1 and its 22G-RNA cofactors are required for holocentric chromosome segregation. *Cell*, **139**, 123-134.
11. Shukla, A., Yan, J., Pagano, D.J., Dodson, A.E., Fei, Y., Gorham, J., Seidman, J.G., Wickens, M. and Kennedy, S. (2020) poly(UG)-tailed RNAs in genome protection and epigenetic inheritance. *Nature*, **582**, 283-288.
12. Preston, M.A., Porter, D.F., Chen, F., Buter, N., Lapointe, C.P., Keles, S., Kimble, J. and Wickens, M. (2019) Unbiased screen of RNA tailing activities reveals a poly(UG) polymerase. *Nat Methods*, **16**, 437-445.
13. Ashe, A., Sapetschnig, A., Weick, E.M., Mitchell, J., Bagijn, M.P., Cording, A.C., Doebley, A.L., Goldstein, L.D., Lehrbach, N.J., Le Pen, J. *et al.* (2012) piRNAs can trigger a multigenerational epigenetic memory in the germline of C. elegans. *Cell*, **150**, 88-99.
14. Towbin, B.D., Gonzalez-Aguilera, C., Sack, R., Gaidatzis, D., Kalck, V., Meister, P., Askjaer, P. and Gasser, S.M. (2012) Step-wise methylation of histone H3K9 positions heterochromatin at the nuclear periphery. *Cell*, **150**, 934-947.

15. Spike, C.A., Bader, J., Reinke, V. and Strome, S. (2008) DEPS-1 promotes P-granule assembly and RNA interference in C. elegans germ cells. *Development*, **135**, 983-993.
16. Kawasaki, I., Shim, Y.H., Kirchner, J., Kaminker, J., Wood, W.B. and Strome, S. (1998) PGL-1, a predicted RNA-binding component of germ granules, is essential for fertility in C. elegans. *Cell*, **94**, 635-645.
17. Ketting, R.F., Haverkamp, T.H., van Luenen, H.G. and Plasterk, R.H. (1999) Mut-7 of C. elegans, required for transposon silencing and RNA interference, is a homolog of Werner syndrome helicase and RNaseD. *Cell*, **99**, 133-141.
18. Batista, P.J., Ruby, J.G., Claycomb, J.M., Chiang, R., Fahlgren, N., Kasschau, K.D., Chaves, D.A., Gu, W., Vasale, J.J., Duan, S. *et al.* (2008) PRG-1 and 21U-RNAs interact to form the piRNA complex required for fertility in C. elegans. *Mol Cell*, **31**, 67-78.
19. Tsai, H.Y., Chen, C.C., Conte, D., Jr., Moresco, J.J., Chaves, D.A., Mitani, S., Yates, J.R., 3rd, Tsai, M.D. and Mello, C.C. (2015) A ribonuclease coordinates siRNA amplification and mRNA cleavage during RNAi. *Cell*, **160**, 407-419.
20. Kennedy, S., Wang, D. and Ruvkun, G. (2004) A conserved siRNA-degrading RNase negatively regulates RNA interference in C. elegans. *Nature*, **427**, 645-649.
21. Tabara, H., Sarkissian, M., Kelly, W.G., Fleenor, J., Grishok, A., Timmons, L., Fire, A. and Mello, C.C. (1999) The rde-1 gene, RNA interference, and transposon silencing in C. elegans. *Cell*, **99**, 123-132.
22. Steiner, F.A., Okihara, K.L., Hoogstrate, S.W., Sijen, T. and Ketting, R.F. (2009) RDE-1 slicer activity is required only for passenger-strand cleavage during RNAi in Caenorhabditis elegans. *Nat Struct Mol Biol*, **16**, 207-211.
23. Phillips, C.M., Montgomery, T.A., Breen, P.C. and Ruvkun, G. (2012) MUT-16 promotes formation of perinuclear mutator foci required for RNA silencing in the C. elegans germline. *Genes Dev*, **26**, 1433-1444.